Related PP2C phosphatases Pic3 and Pic12 negatively regulate immunity in tomato to *Pseudomonas syringae*

Fan Xia[1,2], Ning Zhang[1,2], Renee E. Smith[1], Joydeep Chakraborty[3], Guy Sobol[3], Xuemei Tang[1], Zhangjun Fei[1,2,4], Guido Sessa[3,+], Gregory B. Martin[1,2*]

[1]Boyce Thompson Institute for Plant Research, Ithaca, New York 14853, USA

[2]Plant Pathology and Plant-Microbe Biology Section, School of Integrative Plant Science, Cornell University, Ithaca, New York 14853, USA

[3]School of Plant Sciences and Food Security, The George S. Wise Faculty of Life Sciences, Tel-Aviv University, Tel-Aviv 69978, ISRAEL

[4]USDA-ARS Robert W. Holley Center for Agriculture and Health, Ithaca, New York 14853, USA

[*]Corresponding author: Gregory B. Martin (gbm7@cornell.edu)

[+]Deceased July 4, 2023

ORCID IDs

Fan Xia:	0000-0002-8091-2426
Ning Zhang:	0000-0003-2775-1755
Renee Smith:	0009-0003-5105-9766
Joydeep Chakraborty:	0000-0003-1106-8740
Guy Sobol:	0000-0003-1440-9432
Zhangjun Fei:	0000-0001-9684-1450
Guido Sessa:	0000-0001-8737-7377
Gregory B. Martin:	0000-0003-0044-6830

Abstract

Type 2C protein phosphatases (PP2Cs) constitute a large family in most plant species but relatively few of them have been implicated in immunity. To identify and characterize PP2C phosphatases that affect tomato immunity, we used CRISPR/Cas9 to generate loss-of-function mutations in 11 PP2C-encoding genes whose expression is altered in response to immune elicitors or pathogens. We report that two closely related PP2C phosphatases, Pic3 and Pic12, are involved in regulating resistance to the bacterial pathogen *Pseudomonas syringae* pv. *tomato* (*Pst*). Loss-of-function mutations in *Pic3* lead to enhanced resistance to *Pst* in older but not younger leaves, whereas such mutations in *Pic12* resulted in enhanced resistance in both older and younger leaves. Overexpression of Pic3 and Pic12 proteins in leaves of *Nicotiana benthamiana* inhibited resistance to *Pst* and this effect was dependent on Pic3/12 phosphatase activity and an N-terminal palmitoylation motif associated with localization to the cell periphery. Pic3 but not Pic12 had a slight negative effect on flagellin-associated reactive oxygen species generation, although their involvement in the response to *Pst* appeared independent of flagellin. RNA-sequencing analysis of Rio Grande (RG)-PtoR wild-type plants and two independent RG-pic3 mutants revealed that the enhanced disease resistance in RG-pic3 older leaves is associated with increased transcript abundance of multiple defense related genes. RG-pic3/RG-pic12 double mutant plants exhibited stronger disease resistance than RG-pic3 or RG-pic12 single mutants. Together, our results reveal that Pic3 and Pic12 negatively regulate tomato immunity in an additive manner through flagellin-independent pathways.

Key words: Type 2C protein phosphatases, Plant immunity, *Pseudomonas syringae*, *Solanum lycopersicum,* tomato

66 **Introduction**

67 Plants use a two-layered innate immune system to protect themselves against pathogen attack. The first
68 layer uses cell surface-associated pattern recognition receptor (PRR) proteins to detect pathogen
69 associated molecular patterns (PAMPs) to activate PRR-triggered immunity (PTI). Successful bacterial
70 pathogens translocate effector proteins into plant cells through the type III secretion system (T3SS) and,
71 among several activities, target various host components to inhibit PTI. The second layer of defense
72 deploys intracellular nucleotide-binding, leucine-rich repeat (NLR) family proteins to sense pathogen
73 effectors and initiate effector triggered immunity (ETI) (Jones and Dangl, 2006). Despite the differences
74 in recognition mechanisms, PTI and ETI both elicit some common host responses including reactive
75 oxygen species (ROS) burst and calcium fluxes, activation of mitogen activated protein kinase (MAPK),
76 and transcriptional reprograming and ultimately result in the restriction of pathogen multiplication
77 (Zhang et al., 2020; Wang and Luan, 2023).

78 A well-characterized plant PRR, Flagellin Sensing 2 (Fls2), is a receptor kinase conserved in higher plants
79 that binds a 22 amino acid epitope, flg22, of the bacterial flagellin protein (Sun et al., 2013; Cheng, Xiao
80 and Xiong, 2020). In tomato and other solanaceous plants, a distinct 28 amino acid epitope, flgII-28, also
81 derived from flagellin, is recognized by the receptor kinase Flagellin Sensing 3 (Fls3) (Clarke et al., 2013;
82 Hind et al., 2016). Fls2 and Fls3 each form a complex with co-receptor BRASSINOSTEROID INSENSITIVE
83 1–associated kinase 1 (BAK1) to activate downstream defense responses (Chinchilla et al., 2007; Hind et
84 al., 2016). Fls2- and Fls3-mediated PTI plays an important role in tomato resistance to bacterial
85 pathogens (Rosli et al., 2013; Roberts et al., 2020). Consequently, either the deletion of bacterial
86 flagellin-encoding gene *fliC* or loss-of-function mutations in both Fls2 and Fls3 significantly compromise
87 tomato resistance against *Pseudomonas syringae* pv. *tomato* (*Pst*) DC3000 (Roberts et al., 2020; Zhang
88 et al., 2020). The cold shock protein (CSP)-derived bacterial PAMP, csp22, is recognized by the receptor
89 kinase cold shock protein receptor (CORE) in tomato and loss-of-function mutations in the *CORE* gene in
90 tomato lead to enhanced susceptibility to *Pst* (Danielle et al., 2024).

91 The tomato disease resistance gene *Pto* encodes a protein kinase that physically interacts with T3SS
92 effectors AvrPto and AvrPtoB (Tang et al., 1996; Kim, Lin and Martin, 2002). However, to trigger ETI, Pto
93 interacts and forms a complex with the NLR protein Prf (Ntoukakis et al., 2013). A number of signaling
94 components acting downstream of Pto/Prf have been identified, including NLR required for cell death
95 (Nrc2 and Nrc3), 14-3-3 proteins Tomato Fourteen-Three-three (Tft1, Tft3 and Tft7), mitogen-activated

96 protein (MAP) kinase cascade components MAP Kinase Kinase Kinase (MAPKKKα), MAP kinase kinases
97 (MKK1 and MKK2) and MAP Kinases (wound-inducible protein kinase (WIPK) and NTF6)), and M3Kα-
98 interacting protein 1 (Mai1) (Ekengren et al., 2003; Mucyn et al., 2006; Oh, Pedley and Martin, 2010; Oh
99 and Martin, 2011; Roberts et al., 2019; Sheikh et al., 2023; Zhang et al., 2024). Loss of Pto/Prf or of
100 certain downstream components disrupts Pto/Prf mediated ETI, resulting in compromised resistance
101 against *Pst* stains carrying AvrPto or AvrPtoB.

102 PTI and ETI signaling involve many protein kinases which rely on phosphorylation for promoting signal
103 transduction (Ngou, Ding and Jones, 2022). In contrast, protein phosphatases counteract kinase function
104 by dephosphorylating their substrates. Protein phosphatases together with kinases act as molecular
105 switches and maintain balanced and tightly regulated defense responses (Erickson et al., 2022). For
106 instance, overexpression of kinase associated protein phosphatase (KAPP) in Arabidopsis inhibits the
107 binding of FLS2 with flagellin and results in reduced flagellin sensitivity (Gomez-Gomez, Bauer and
108 Boller, 2001). A heterotrimeric protein Ser/Thr phosphatase type 2A (PP2A), comprised of several
109 subunits, has been shown to regulate Arabidopsis immunity through modulating the phosphorylation
110 status of FLS2 co-receptor BAK1 (Segonzac et al., 2014). Additionally, silencing a catalytic subunit of
111 PP2A (PP2Ac) in *Nicotiana benthamiana* reduces PP2A activity and enhances the hypersensitive
112 response (HR) induced by avirulent *Pst* (He et al., 2004).

113 In Arabidopsis, there are about 1,125 protein kinases but only around 150 protein phosphatases (Bheri
114 et al., 2021). Notably, much less is known about protein phosphatases than kinases in plant defense,
115 partly because forward genetic screening of defense-related mutants in the past has rarely identified
116 protein phosphatases (He et al., 2004). Based on protein sequence and catalytic mechanism, plant
117 protein phosphatases are divided into four families: phosphoprotein phosphatase (PPP), protein
118 phosphatase 2C (PP2C, also named Mg^{2+}/Mn^{2+}-dependent protein phosphatase (PPM)),
119 phosphotyrosine phosphatase (PTP) and Asp-dependent phosphatase (Uhrig, Labandera and Moorhead,
120 2013). The PPP and PP2C family members are serine/threonine protein phosphatases that
121 dephosphorylate phospho-serine and phospho-threonine but the sequences of PP2Cs are distinct from
122 those of PPP members (Uhrig, Labandera and Moorhead, 2013). Significant attention has been given to
123 PP2Cs in recent years as many of them are found to regulate biotic and abiotic stresses (Schweighofer,
124 Hirt and Meskiene, 2004; Sobol et al., 2022). For example, several PP2Cs are regulators of abscisic acid
125 (ABA) signaling, which plays an important role in abiotic stress responses and other physiological
126 processes (Chen et al., 2020). In Arabidopsis, several PP2C phosphatases have been implicated in

127 dampening immunity by dephosphorylating defense signaling components. These include Highly ABA-
128 Induced1 (HAI1) and Arabidopsis PP2C-type phosphatase 1 (AP2C1) that dephosphorylate MAPKs and
129 PP2C38 that dephosphorylates Botrytis-Induced Kinase 1 (BIK1), POLTERGEIST-LIKE 4 (PLL4) that
130 mediates dephosphorylation of FLS2 and the Elongation Factor Tu Receptor (EFR), and chitin elicitor
131 receptor kinase1 (CERK1)-interacting protein phosphatase 1 (CIPP1) that dephosphorylates chitin co-
132 receptor CERK1 (Schweighofer et al., 2007; Couto et al., 2016; Mine et al., 2017; Liu et al., 2018; DeFalco
133 et al., 2022). In rice, PP2C phosphatase XA21 binding protein 15 (XB15) mediates receptor kinase XA21
134 dephosphorylation and the loss of XB15 activates cell death, increases defense-related gene expression,
135 and enhances XA21-mediated resistance (Park et al., 2008).

136 Most research about plant PP2Cs has been performed in Arabidopsis and to a lesser extent in rice. Little
137 is known about the role of these phosphatases in the tomato immune response. Compared to
138 Arabidopsis and rice, which have 80 and 76 PP2C phosphatases, respectively, the tomato (*Solanum*
139 *lycopersicum*) genome encodes 97 PP2C phosphatases (Xue et al., 2008; Fuchs et al., 2013; Qiu et al.,
140 2022; Sobol et al., 2022). Many tomato PP2Cs share high sequence similarity with their Arabidopsis and
141 rice counterparts, suggesting they might play a conserved role in these species. We previously reported
142 that the tomato PP2C phosphatase Pic1 negatively modulates ROS production in *N. benthamiana* by
143 dephosphorylating a key PTI related kinase, Pti1b (Schwizer et al., 2017; Giska and Martin, 2019). By
144 examining transcriptomic data, we subsequently found that transcript abundances of *Pic1* and 12 other
145 tomato PP2C genes were significantly increased or decreased upon PAMP and pathogen treatments,
146 suggesting they might have a role in immunity (Sobol et al., 2022). We now refer to these as PP2C
147 immunity-associated candidate (Pic) proteins. Here we used CRISPR/Cas9 technology to generate
148 mutations in a collection of *Pic* genes and report that two closely related Pic phosphatases negatively
149 regulate tomato immunity.

150 **Results**

151 **A screen of PP2C immunity candidate (Pic) mutant lines reveals that Pic3 negatively regulates**
152 **resistance to *P. syringae* pv. *tomato* in older but not younger leaves**

153 To assess the role of Pic phosphatases in the tomato defense response, we first generated gene-specific
154 guide RNAs (gRNAs) and used CRISPR/Cas9 technology to induce loss-of-function mutations in a set of
155 eight previously identified PP2C-encoding genes and, in two cases (*Pic7* and *Pic10*), an additional two
156 closely-related genes (Sobol et al., 2022) (**Figure 1A** and **Supplemental Figure S1**). Agrobacterium-
157 mediated stable transformation with the 10 gRNA constructs was performed using tomato cultivar Rio-

158 Grande PtoR (RG-PtoR, wildtype), which expresses the *Pto/Prf* genes and recognizes race 0
159 *Pseudomonas syringae* pv. *tomato (Pst)* strains (Pedley and Martin, 2003). Cas9-mediated target gene
160 disruption resulted in deletions and insertions near the 5' end of the *Pic* genes, which caused open-
161 reading frameshifts and introduced a premature stop codon (except for *Pic11*), leading to predicted loss-
162 of-function mutations (**Figure 1A** and **Supplemental Figures S1** and **S2A**). For most *Pic* genes, we
163 obtained multiple transgenic lines (referred to as RG-pic lines) and chose 1 or 2 independent lines for
164 each gene for further study. The overall morphology and growth of 4-week-old RG-pic mutant plants
165 was generally indistinguishable from wild-type plants (**Figure 1A** and **Supplemental Figure S3A**).

166 To test if these *Pic* genes are involved in tomato defense responses to *Pst*, we inoculated each RG-pic
167 line with three different *Pst* DC3000 strains. DC3000Δ*avrPto*Δ*avrPtoB* (DC3000ΔΔ) carries deletions in
168 two genes encoding type III effectors that are recognized by Pto/Prf (Lin and Martin, 2005). Thus, it does
169 not trigger ETI and can be used to test PTI-based responses in RG-PtoR plants. The
170 DC3000Δ*avrPto*Δ*avrPtoB*Δ*fliC* (DC3000ΔΔΔ) strain, has an additional deletion of the *fliC* gene encoding
171 the flagellin protein. Since flagellin-associated peptides, flg22 and flgII-28, are the major *Pst* PAMPs
172 recognized by tomato (via the Fls2 and Fls3 receptors, respectively), this strain can reveal potential non-
173 flagellin-based basal defense responses in tomato (Rosli et al., 2013; Hind et al., 2016; Roberts et al.,
174 2020). The wild-type DC3000 strain is used to test for AvrPto- and AvrPtoB-activated ETI responses
175 (Zhang et al., 2020). Our screening of the RG-pic mutant lines showed that loss-of-function mutations in
176 nine of the *Pic* genes (two genes each in the RG-pic7 and RG-pic10 lines) did not significantly affect the
177 tomato response to any of the DC3000 strains, as bacterial populations in these RG-pic mutants were
178 not statistically different from wild-type plants (**Supplemental Figures S3B, S3C** and **S3D).**

179 Two independent lines were identified that had predicted loss-of-function mutations in the *Pic3* gene
180 (Solyc01g105280). Line RG-pic3-1 has a 17-bp deletion and 4-bp substitutions in exon 2 and line RG-pic3-
181 2 has a 4-bp deletion in exon 2 (**Figure 1A**). In both cases, the mutations are predicted to result in
182 truncated proteins lacking the PP2C domain (**Supplemental Figure S2A**). Inoculation of the lines with
183 DC3000ΔΔ resulted in fewer bacterial specks in the older leaves of the RG-pic3 lines than on wild-type
184 plants at 4 days after inoculation (**Figure 1B**). In addition, lower bacterial populations were observed in
185 older leaves of the RG-pic3 lines than in wild-type plants at 2 days post-inoculation (dpi; **Figure 1B**).
186 Interestingly, DC3000ΔΔ disease symptoms and populations in younger leaves of the RG-pic3 mutant
187 lines were not different from those of wild-type plants (**Figure 1B**).

188 When inoculated with DC3000ΔΔΔ, we observed less severe disease symptoms and markedly reduced
189 bacterial population in older leaves of both RG-pic3 lines compared to wild-type plants, while
190 DC3000ΔΔΔ disease symptoms and populations in younger leaves were not different between wild-type
191 and RG-pic3 plants (**Figure 1C**). These results suggest that Pic3 negatively regulate PTI and/or other basal
192 defenses, and this regulation is at least partially independent of flg22 and flgII-28. Since both RG-pic3-1
193 and RG-pic3-2 showed similar phenotypes in these initial experiments we used just the RG-pic3-1 line in
194 some of the subsequent experiments.

195 As expected, DC3000 at a relatively low titer ($2x10^5$ cfu/mL) activates ETI and did not cause symptoms
196 on wild-type RG-PtoR plants, but bacterial populations in this line still slightly increased at 2 dpi. The RG-
197 pic3 plants supported slightly less DC3000 growth than wild-type plants in the older but not younger
198 leaves (**Figure 1D**). However, RG-pic3 plants inoculated with a higher titer of DC3000 ($1x10^7$ cfu/mL)
199 developed a hypersensitive response that was indistinguishable from wild-type RG-PtoR plants
200 (**Supplemental Figure S4**), indicating that Pic3 does not play a major role in regulating ETI. Finally, we
201 observed that older leaves of 8-week-old plants of the two RG-pic3 lines started to show early
202 senescence while those of wild-type plants did not (**Supplemental Figure S2B**), suggesting an
203 autoimmune response or Pic3-mediated regulation of additional processes in addition to defense.

204 Pic3 protein belongs to clade D or clade F of PP2Cs, depending on the phylogenetic analysis (Fuchs et al.,
205 2013; Qiu et al., 2022; Sobol et al., 2022). Several clade A PP2Cs have been reported to regulate ABA
206 signaling, which in some cases is involved in senescence development (Tischer et al., 2017; Chen et al.,
207 2020). To test if the enhanced disease resistance seen in RG-pic3 plants might be associated with an
208 ABA response, we examined the expression of two well-known ABA-pathway reporter genes in RG-pic3
209 plants after exogenous ABA treatment (Ma et al., 2018; Lei et al., 2023). The expression levels of these
210 two genes, *AREB1* and *SAG113*, were not different in RG-pic3 plants compared to wild-type plants
211 (**Supplemental Figures S5A** and **S5B**), suggesting Pic3-associated defense is unlikely to be associated
212 with an ABA response.

213 **Pic3 phosphatase activity and its palmitoylation motif are required for its negative regulation of the**
214 **tomato immune response**

215 *Pic3* encodes a PP2C protein with a single PP2C catalytic domain but no known regulatory domain at the
216 N and C terminus (Sobol et al., 2022). The catalytic domain contains conserved aspartic acid residues
217 that play a role in binding metal ions such as Mn^{2+}/Mg^{2+} (**Supplemental Figure S6**), and several studies

218 (Jackson, Fjeld and Denu, 2003; Conner et al., 2006; Couto et al., 2016; Giska and Martin, 2019) reported
219 that substitutions from aspartic acid (D) to asparagine (N) at these highly conserved sites abolishes
220 phosphatase activities. To test the possible requirement of Pic3 phosphatase activity in defense, we
221 generated a construct carrying a variant, Pic3NN, with substitutions at the two conserved aspartic
222 residues (D71N and D233N; **Figure 2A**). Using the 'agromonas' approach (Buscaill et al., 2021), we
223 transiently expressed Pic3, Pic3NN and a YFP control for 2 days in *N. benthamiana* leaves and then
224 inoculated the plants with DC3000*ΔhopQ1-1,* which lacks the T3SS effector gene *hopQ1-1* that can be
225 detected by the NLR protein Recognition of XopQ 1 (Roq1), thus making DC3000*ΔhopQ1-1* virulent in *N.*
226 *benthamiana;* (Wei et al., 2007; Schultink et al., 2017). Compared to the YFP control, transient
227 expression of wild-type Pic3 significantly increased the DC3000*ΔhopQ1-1* population in *N. benthamiana,*
228 consistent with Pic3 playing a negative role in resistance to DC3000*ΔhopQ1-1* (**Figure 2B**). In contrast,
229 bacterial abundance in leaves expressing Pic3NN were not statistically different from that in plants
230 expressing YFP (**Figure 2B**), indicating that phosphatase activity plays an important role in Pic3 function
231 in defense. Consistent with the observation that Pic3-modulated defense is flagellin independent, when
232 inoculated with a flagellin deficient strain, DC3000*ΔhopQ1-1ΔfliC*, *N. benthamiana* plants expressing
233 wild-type Pic3 protein also supported significantly higher bacterial populations than plants expressing
234 Pic3NN or YFP (**Figure 2C**). Immunoblot analysis confirmed that the Pic3 and Pic3NN proteins were
235 expressed in leaves at similar levels (**Figure 2D**).

236 We next discovered, using GS-Palm (Ning et al., 2021), that three cysteine residues (C5, C6 and C21) at
237 the Pic3 N- terminus constitute a predicted palmitoylation motif. Palmitoylation is the covalent addition
238 of fatty acids to a cysteine residue, which often promotes association of proteins with membranes (Lin,
239 2021). As our disease assays indicate that Pic3 could negatively regulate a PTI response, we
240 hypothesized that Pic3 might associate with the plasma membrane to modulate early PTI-related
241 signaling events. To test the possible requirement of Pic3 palmitoylation in defense, we generated a
242 construct carrying a Pic3 variant with a disrupted palmitoylation motif (Pic3SSS; with C5S, C6S and C21S
243 substitutions) and tested it using the agromonas approach described above (**Figures 2A, 2B** and **2C**). We
244 observed that bacterial abundances in Pic3SSS-expressing plants were not statistically different from
245 those in plants expressing YFP or Pic3NN (**Figures 2B** and **2C**), suggesting that palmitoylation is required
246 for Pic3 function in defense. Immunoblot analysis confirmed that the Pic3 and Pic3SSS proteins were
247 expressed at similar levels (**Figure 2D**).

248 To test if the palmitoylation motif affects Pic3 subcellular localization, we fused a YFP tag to the C-
249 terminus of Pic3 and Pic3SSS and examined Pic3- and Pic3SSS-YFP fusion protein localization with a
250 confocal microscope. As expected, we found that fluorescence from the YFP protein control was present
251 in both the cytosol and nucleus. Fluorescence from the Pic3-YFP protein was noticeably associated with
252 the cell periphery, whereas a significant portion of Pic3SSS-YFP fluorescence appeared in the nucleus
253 (**Figure 2E**). Immunoblot analysis confirmed that the Pic3-YFP and Pic3SSS-YFP proteins were expressed
254 at similar levels (**Supplemental Figure S7A**). These observations support the hypothesis that
255 palmitoylation of the Pic3 protein affects its subcellular localization. We also investigated, but did not
256 find, an effect on Pic3 protein localization associated with inoculation by DC30000*ΔhopQ1-1* or exposure
257 to the PAMP flg22 (**Supplemental Figure S7B**).

258 **Pic3 does not affect MAPK activation but has a minor role in negatively regulating flgII-28 mediated**
259 **ROS production**

260 MAPK activation and ROS production are two PTI-associated responses that occur in tomato after the
261 recognition of flg22 or flgII-28 by Fls2 or Fls3, respectively (Roberts et al., 2020; Zhang et al., 2020).
262 Although we showed that Pic3-modulated defense against *Pst* can be independent of flagellin, it
263 remained possible that certain responses controlled by Fls2 and/or Fls3 might be regulated by this
264 phosphatase. We therefore monitored MAPK activation in wild-type and RG-pic3 plants after exposure
265 to flg22 or flgII-28 (Chinchilla et al., 2006; Hind et al., 2016; Roberts et al., 2020). We also included in our
266 MAPK assay another PAMP, csp22 peptide, which is derived from a cold shock protein, and recognized
267 by the CORE receptor (Wang et al., 2016; Danielle et al., 2024) to see if it was involved in the flagellin-
268 independent response we observed earlier. MAPKs were activated similarly in both older and younger
269 leaves in wild-type and RG-pic3 plants with all three different peptide treatments (**Figure 3A**). Other
270 unknown PAMPs might also induce PTI and trigger MAPK activation in tomato. To test if MAPK
271 activation due to these PAMPs is affected by Pic3, we used boiled *Pst* cell lysates from DC3000ΔΔ and
272 DC3000ΔΔΔ as a source of other unknown PAMPs to induce MAPK. However, we again detected no
273 significant difference between RG-pic3 and wild-type plants in MAPK activation in response to these
274 lysates (**Supplemental Figure S8**).

275 To test if Pic3 affects Fls2- or Fls3-mediated ROS production, we measured ROS production in older and
276 younger leaves of RG-pic3 and wild-type plants after flg22 or flgII-28 treatment. We observed no
277 statistically significant increase in flg22-induced ROS in older leaves of RG-pic3 compared to wild-type
278 plants (**Figure 3B**). However, after flgII-28 treatment, older leaves of RG-pic3 plants did consistently

279 show higher ROS production than those of wild-type plants (**Figure 3C**). We observed no difference in
280 ROS production in younger leaves between RG-pic3 and wild-type plants in response to either flg22 or
281 flgII-28 (**Figures 3D** and **3E**). Overall, these results suggest that Pic3 has a slight negative effect on flgII-
282 28-activated ROS production but otherwise does not have a detectable effect on two well-characterized
283 PTI responses.

284 **Transcript abundance of defense-related genes in RG-pic3 plants is increased in older leaves compared**
285 **to wild-type plants**

286 *Pst* is known to activate significant transcriptional reprograming in tomato, which is associated with
287 restriction of bacterial multiplication in leaves (Rosli et al., 2013; Pombo et al., 2014; Zhang et al., 2022).
288 To investigate how Pic3 might affect the plant immune response independent of flagellin, we vacuum
289 inoculated wild-type plants and the two RG-pic3 lines with DC3000ΔΔΔ and collected RNA samples from
290 older leaves and younger leaves separately at 6 h post-inoculation (hpi) and carried out an RNA-
291 sequencing (RNA-Seq) analysis. This analysis revealed that substantially more differently expressed
292 genes (DEGs) were found in older than younger leaves of RG-pic3 compared to wild-type plants (**Figure**
293 **4A**). As we have done previously to simplify the analysis (Rosli et al., 2013; Pombo et al., 2014), we
294 focused on genes with an FPKM (fragments per kilobase of transcript per million mapped fragments) of
295 ≥3 in RG-pic3 (for up-regulated DEGs) or wild-type plants (for down-regulated DEGs), and a fold-change
296 of ⩾2 and an FDR (false discovery rate) of < 0.05. Applying these parameters to older leaves, we found
297 that transcript abundance of 1,123 genes was greater in RG-pic3 plants compared to wild-type plants
298 and transcript abundance of 387 genes was less in RG-pic3 compared to wild-type plants (**Figure 4A**). In
299 contrast, in younger leaves there were only 13 genes with higher transcript abundance in RG-pic3
300 compared to wild-type plants and just two genes with lower transcript abundance in RG-pic3 compared
301 to wild-type plants. These results are consistent with the observation that RG-pic3 plants have stronger
302 resistance to DC3000ΔΔΔ than wild type plants in older but not in younger leaves (**Figure 1C**).

303 Transcript abundance of several genes associated with PTI was higher in older leaves of RG-pic3
304 compared to wild-type (**Figure 4B**), and it is possible that the increased expression of these genes
305 contributes to the enhanced resistance in RG-pic3 older leaves. To gain broader insight into how the
306 1,123 upregulated DEGs might impact the enhanced resistance in RG-pic3 older leaves, we conducted a
307 gene ontology (GO) analysis. GO terms associated with 69 biological processes, 6 cellular components
308 and 54 molecular functions were significantly enriched in the upregulated DEGs in older leaves
309 (**Supplemental Table S1A**; FDR < 0.05). GO terms in the biological processes and molecular function

310 categories with the lowest FDR were related to defense responses and protein phosphorylation,
311 respectively (**Figure 4C**), supporting the idea that Pic3 might regulate immunity by catalyzing
312 dephosphorylation reactions. GO terms in the cellular component category with lowest FDR were
313 related to subcellular localization that is consistent with our observation of Pic3 at the cell periphery
314 (**Figure 4C**). In contrast, many of the enriched GO terms in downregulated DEGs in older leaves were
315 related to photosynthesis (**Figure 4D** and **Supplemental Table S1B**). These results are not unexpected as
316 photosynthesis and growth are known to be downregulated when plants allocate more resource for
317 defense signaling (Bolton, 2009; Su et al., 2018).

318 We next sought to determine if certain individual upregulated DEGs significantly contribute to the
319 enhanced resistance in older leaves of RG-pic3. We narrowed our focus for such genes to the 105 most
320 highly upregulated DEGs in RG-pic3 older leaves (fold change ≥10, FDR < 0.05). Among these 105 genes,
321 a cluster of genes (*Solyc12g100240*, *Solyc12g100250*, *Solyc12g100270* and *Solyc12g049030*) involved in
322 defense-related fatty acid biosynthesis (Jeon et al., 2020) and several other potential defense related
323 genes were selected for functional analysis (**Supplemental Table S2**). We used the agromonas approach
324 to test the possible contribution of 11 of these genes to defense by overexpressing them in *N.*
325 *benthamiana* and measuring the response to DC30000*ΔhopQ1-1ΔfliC.* None of the genes altered *N.*
326 *benthamiana* resistance to DC30000*ΔhopQ1-1ΔfliC* (**Supplemental Figure S9**), suggesting the enhanced
327 resistance in RG-pic3 older leaves is likely due to the combined effect of multiple genes/defense
328 responses.

329 We found that the transcript abundance of *Bti9*, which encodes a lysin motif (LysM) receptor-like kinase
330 (AvrPtoB tomato-interacting 9), is increased in older leaves of the RG-pic3 mutants compared to wild-
331 type plants after DC3000ΔΔΔ inoculation (**Figure 4B)**. The Bti9 protein has the highest sequence identity
332 among tomato LysM-RLKs with the Arabidopsis chitin co-receptor CERK1 and is required for resistance
333 to *P*. *syringae* and *Botrytis cinerea* (Zeng et al., 2012; Jaiswal et al., 2022). The closest Pic3 homolog
334 protein in Arabidopsis is CIPP1, which is known to negatively regulate immunity by dephosphorylating
335 CERK1 (Liu et al., 2018). To test if Pic3 might regulate *Pst* resistance through Bti9, we crossed a loss-of-
336 function RG-bti9 mutant with the RG-pic3-1 mutant and generated an RG-pic3/bti9 double mutant.
337 Upon inoculation with DC3000ΔΔΔ, the RG-bti9-1 mutant had more severe disease symptoms and
338 slightly higher bacterial growth in older leaves than wild-type plants although the difference in bacterial
339 populations in some experiments was not statistically significant (**Supplemental Figures S10A, S10B**,
340 **S10C** and **S10D**). Importantly, the loss-of-function mutation in *Bti9* did not significantly compromise the

341 increased resistance in lower leaves to DC3000ΔΔΔ in the RG-pic3/RG-bti9 plants (**Supplemental Figures**
342 **S10A, S10B, S10C** and **S10D**). In addition, co-expression of Bti9 and Pic3 in leaves of *N. benthamiana* did
343 not show any evidence of Pic3 affecting Bti9 phosphorylation during defense activation (**Supplemental**
344 **Figure S11**). We therefore conclude that Bti9 does not play a detectable role in Pic3-modulated
345 immunity to *Pst*.

346 **Another PP2C phosphatase, Pic12, is closely related to Pic3 and also negatively regulates the tomato**
347 **immune response**

348 In a review of our earlier RNA-Seq data (Rosli et al., 2013; Pombo et al., 2014), we noticed that the *Pic3*
349 gene has a remarkably similar pattern of expression during the tomato PTI and ETI responses as another
350 PP2C gene, *Pic12* (Solyc10g047290; **Supplemental Table S3**). This was also the case for their expression
351 in response to the flagellin-deficient strain DC3000ΔΔΔ in both older and younger leaves (**Supplemental**
352 **Figures S12A** and **S12B).** Interestingly, the Pic3 and Pic12 proteins share 84% amino acid identity and,
353 are closely related to Arabidopsis CIPP1 and a defense-related PP2C (Os04g37904) in rice (Wang et al.,
354 2012) (**Supplemental Figures S12C** and **S12D**). Together, these observations raised the possibility that
355 Pic3 and Pic12 might have overlapping defense functions in tomato.
356
357 To investigate the role of Pic12 in the tomato defense response, we used the CRISPR/Cas9 approach
358 described above, to generate two independent RG-pic12 homozygous mutant lines (**Figure 5A**). Both
359 lines have mutations in the second exon of the *Pic12* gene with one (RG-pic12-1) having a 14 bp deletion
360 and the other (RG-pic12-2) a 1 bp insertion. Each mutation causes a shift in the open reading frame
361 resulting in predicted truncated proteins lacking the PP2C domain (**Figure 5A** and **Supplemental Figure**
362 **S13A).** The RG-pic12 mutant plants had wild-type morphology at 4 weeks old (**Figure 5A**). At 8 weeks
363 old, the RG-pic12 plants were slightly shorter than wild-type and at 12 weeks old the plants showed
364 earlier senescence than wild-type (**Supplemental Figures S13B** and **S13C**).
365
366 We tested defense-related responses of the RG-pic12 plants by inoculating them and wild-type plants
367 with the three *Pst* DC3000 strains described earlier. Unlike the RG-pic3 mutant lines, the two RG-pic12
368 lines showed increased resistance to DC3000ΔΔ and DC3000ΔΔΔ in both older and younger leaves, as
369 shown by less disease symptoms and lower bacterial populations (**Figures 5B** and **5C**). Disease
370 symptoms and bacterial populations in RG-pic12 and wild-type plants after inoculation with DC3000

371 were similar (**Figure 5D).** Together, these observations suggest that Pic12, like Pic3, regulates flagellin-
372 independent defense responses but does not appear to affect Pto/Prf-mediated ETI.

373 The Pic12 protein has two cysteines (C5 and C6) that are predicted to be palmitoylated and two
374 conserved aspartic acids (D69 and D231) expected to be required for its phosphatase activity
375 (**Supplemental Figure S14A**). To test the importance of these residues, we made serine substitutions for
376 the two cysteines (C5S and C6S; Pic12SS) and asparagine substitutions for the two aspartic acid residues
377 (D69N and D231N; Pic12NN). The wild-type Pic12 and each variant were transiently expressed in leaves
378 of *N. benthamiana* and the effect on subsequent inoculation with DC3000*ΔhopQ1-1ΔfliC* was measured.
379 Expression of wild-type Pic12 but not Pic12SS or Pic12NN increased *N. benthamiana* susceptibility to
380 DC3000*ΔhopQ1-1ΔfliC* relative to a YFP control (**Figure 5E**). An immunoblot showed that all proteins
381 were expressed at a similar level (**Figure 5F**). These data indicate that like Pic3, the palmitoylation motif
382 and phosphatase activity are required for Pic12-mediated negative regulation of plant defense.

383 **Pic12 is localized to the cell periphery and does not affect flagellin-induced MAPK activation or ROS**
384 **production**

385 Because the substitutions in the Pic12 palmitoylation motif compromised its defense function, we
386 hypothesized that, like with Pic3, this motif is required for Pic12 subcellular localization. We fused wild-
387 type Pic12 and Pic12SS to a C-terminus YFP tag and visualized their localization in the plant cell by
388 transiently expressing each protein (along with a YFP control) in leaves of *N. benthamiana*
389 (**Supplemental Figure S14B**). Like Pic3, wild-type Pic12-YFP protein was primarily localized to cell
390 periphery. However, the Pic12-YFP fluorescence at the periphery largely disappeared in leaves
391 expressing Pic12SS-YFP (**Supplemental Figure S14B**), suggesting the palmitoylation motif is required for
392 proper localization of Pic12. An immunoblot showed that all proteins were expressed in these
393 experiments, though Pic12-YFP was less abundant (**Supplemental Figure S14C**). As with Pic3, Pic12
394 localization was not changed after DC3000*ΔhopQ1-1* inoculation or flg22 treatment (**Supplemental**
395 **Figure S14D**).

396 To test if Pic12 plays a role in flagellin-mediated PTI, we measured MAPK activation and ROS production
397 in older and younger leaves of RG-pic12 and wild-type plants after either flg22 or flgII-28 treatment. We
398 observed similar levels of MAPK activation and ROS production in both RG-pic12 and wild-type plants in
399 these experiments (**Supplemental Figures S15A**, **S15B**, and **S15C**). Pic12 therefore does not appear to
400 regulate two host responses associated with flagellin-mediated PTI.

401

402 **Pic3 and Pic12 negatively regulate resistance to another bacterial pathogen, *Xanthomonas***
403 ***euvesicatoria***

404 Our experiments to this point had focused on the response of the RG-pic3 and RG-pic12 mutants to
405 different strains of DC3000 and supported a role of both PP2Cs in the negative regulation of plant
406 defenses against this bacterial pathogen. To extend these observations beyond *Pst*, we inoculated RG-
407 pic3, RG-pic12 and wild-type plants with another bacterial foliar pathogen, *Xanthomonas euvesicatoria*
408 (*Xe*), the causative agent of bacterial spot disease of tomato and measured bacterial populations in
409 older and younger leaves. Like the responses to *Pst*, RG-pic3 plants showed enhanced resistance in older
410 leaves to *Xe*, while RG-pic12 plants showed enhanced resistance to this pathogen in both older and
411 younger leaves (**Supplemental Figure S16**).

412 **Pic3 and Pic12 additively contribute to bacterial disease resistance in tomato**

413 Except for the RG-pic3 mutants showing enhanced resistance only in older leaves compared to the
414 enhanced resistance in both older and younger leaves of RG-pic12 plants, similar phenotypes of the
415 mutant lines, the relatedness of the Pic3 and Pic12 proteins, and their similar gene expression patterns
416 suggested that the two PP2Cs might have at least partially redundant/additive functions in negatively
417 regulating flagellin-independent immunity. To test this possibility, we crossed RG-pic3-1 and RG-pic12-2
418 to generate an RG-pic3/RG-pic12 double mutant. The double mutant began to show altered morphology
419 at 4 weeks-old with noticeably deformed older leaves (**Figure 6A**). At 8 weeks-old, leaves of RG-pic3/RG-
420 pic12 plants showed pronounced early senescence compared to wild-type and single RG-pic3 or RG-
421 pic12 plants (**Figure 6A**) and they produced very few viable seeds. Upon inoculation with DC3000ΔΔΔ,
422 RG-pic3/RG-pic12 plants supported smaller bacterial populations in older leaves than the RG-pic3 or RG-
423 pic12 single mutants, although disease symptoms in the RG-pic12 plants were as severe as in wild-type
424 plants with this DC3000 strain (**Figures 6B** and **6C**). In younger leaves the RG-pic3/RG-pic12 and RG-
425 pic12 plants both supported lower bacterial populations and showed less severe disease symptoms
426 (**Figures 6B** and **6C**). Collectively, with respect to bacterial growth, these observations indicate that in
427 older leaves Pic3 and Pic12 act in a partially redundant manner, whereas in younger leaves Pic12 acts
428 without Pic3. MAPK activation after flg22 or flgII-28 treatment in RG-pic3/RG-pic12 plants was not
429 different from wild-type or RG-pic3 or RG-pic12 single mutant plants in older and younger leaves
430 (**Supplemental Figure S17**), further indicating that neither Pic3 nor Pic12 affect this flagellin-associated
431 PTI response.

432 **Discussion**

433 Protein phosphorylation is a reversable posttranslational modification that can regulate protein
434 conformation, stability, activity, and localization. In many biological processes, protein kinases and
435 phosphatases act as a molecular switch by turning protein phosphorylation 'on' and 'off' (Zhang et al.,
436 2023). In defense responses, plants rely on transmembrane cell-surface and intracellular receptors to
437 sense the presence of pathogens. Many of the surface receptors have an intracellular protein kinase
438 domain and they transduce outside stimuli into coordinated cellular responses by phosphorylating
439 specific substrates (Bi et al., 2018; DeFalco and Zipfel, 2021). As the environment changes, plants adjust
440 their responses by modulating cellular protein phosphorylation status via protein phosphatases
441 (Erickson et al., 2022; Sobol et al., 2022). Similarly, some intracellular NLR receptors rely on protein
442 kinases to activate robust immune responses upon recognition of specific pathogen 'effector' proteins
443 (del Pozo, Pedley and Martin, 2004; Pedley and Martin, 2004; Roberts et al., 2019; Zhang and Zhang,
444 2022). While much progress has been made in understanding the role of protein kinases in plant
445 immunity, less is known about how protein phosphatases regulate defense signaling. PP2C protein
446 phosphatases constitute a large family in plants and a few studies have shown them to play a role in
447 plant immunity (Schweighofer et al., 2007; Park et al., 2008; Couto et al., 2016; Giska and Martin, 2019).
448 In this study, we used CRISPR/Cas9 gene editing technology in tomato to generate loss-of-function
449 mutations in a collection of PP2C-immunity associated candidate (Pic) genes and investigated their
450 possible roles in bacterial resistance. We discovered and characterized two PP2Cs that negatively
451 regulate the plant immune response in a leaf age-specific manner.

452 Our screening of the Pic mutants for their response to three *Pst* DC3000 strains led us to discover two
453 PP2C phosphatases, Pic3 and Pic12, that negatively regulate disease resistance to two different bacterial
454 pathogens. Interestingly, the enhanced resistance in RG-pic3 (but not RG-pic12) plants is observed only
455 in older leaves and not in younger leaves. Consistent with this observation, our RNA-seq analysis of RG-
456 pic3 vs. wild-type plants revealed significantly more DEGs in older than in younger leaves. This
457 difference in older and younger leaves is reminiscent of the leaf age-dependent response to *Pst* DC3000
458 seen in Arabidopsis *fls2* mutants (Zipfel et al., 2004). In that case, the *fls2* mutant plants show increased
459 disease susceptibility in younger leaves as compared to older leaves (Zipfel et al., 2004). However, the
460 different disease symptoms seen in older and younger leaves of the RG-pic3 lines is not likely to involve
461 Fls2 (or Fls3) because RG-pic3 plants also show enhanced resistance in older leaves to DC3000ΔΔΔ,
462 which does not produce flagellin. In addition, MAPK activation and ROS production were mostly similar

463 in RG-pic3, RG-pic12 and wild-type plants after various PAMP treatments, further indicating that the two
464 phosphatases do not have a significant effect on flagellin-activated defense pathways.

465 The localization of Pic3 and Pic12 at the cell periphery suggests that they might regulate defense
466 responses by dephosphorylating immunity-associated proteins near plasma membrane. The GO term
467 analysis showed clear enrichment for terms such as “membrane”, “phosphorylation”, and “defense” in
468 the upregulated DEGs in older leaves of RG-pic3 vs. wild-type plants, further supporting this hypothesis.
469 We used the agromonas assay to investigate the role of some of these upregulated DEGs in the Pic3-
470 mediated response. However, overexpression of 11 individual candidate genes (selected from 105 DEGs
471 with highest fold change) did not alter resistance to DC3000 in leaves of *N. benthamiana*. Although we
472 do see an effect on DC3000 when Pic3 and Pic12 are used in the agromonas assay, it seems likely that
473 the enhanced defense seen in older leaves of RG-pic3 plants is due to the upregulation of an array of
474 genes working synergistically or additively. Our RNA-seq data did show that several known PTI-
475 associated genes are among the upregulated DEGs in older RG-pic3 leaves, and one or more of these
476 genes could conceivably contribute to the enhanced resistance we observed.

477 Pic3 and Pic12 share similarities in amino acid sequence, gene expression pattern, localization, and both
478 negatively regulate defense in a flagellin independent manner. However, there is evidence that Pic3 has
479 a slightly different regulatory role than Pic12. First, RG-pic3 mutants show increased resistance only in
480 older leaves whereas RG-pic12 mutants exhibit enhanced resistance in both older and younger leaves.
481 Second, RG-pic3, but not RG-pic12, mutants show slightly enhanced resistance to DC3000. Third, the RG-
482 pic3, but not RG-pic12, plants develop early senescence when they are two-months old. Fourth, flgII-28
483 induced ROS is higher in older leaves of RG-pic3 than in wild-type plants, while Pic12 does not have an
484 effect on flgII-28 induced ROS. Fifth, the RG-pic3/RG-pic12 plants show a stronger resistance to
485 DC3000ΔΔΔ than the RG-pic3 or RG-pic12 single mutants. Interestingly, the pronounced spontaneous
486 cell death seen in unchallenged RG-pic3/RG-pic12 plants is not seen in RG-pic3 or RG-pic12 single
487 mutants. Collectively, these observations suggest that Pic3 and Pic12 act in at least a partially redundant
488 fashion and conceivably target some common and some different substrates to regulate defense
489 responses.

490 Phylogenetic analysis of Pic3, Pic12 and related PP2C phosphatases revealed that Pic3 and Pic12 (along
491 with Solyc04g074190, but this gene was not induced after PAMP treatments) are closely related to
492 *Arabidopsis* phosphatases AtCIPP1 and AtPAPP2C, as well as rice Os04g37904 (**Supplemental Figure**

493 **S12C**). CIPP1 has been shown to negatively regulate defense by dephosphorylating CERK1, and both
494 AtPAPP2C and Os04g37904 have been implicated in regulating salicylic acid (SA)-dependent immunity
495 (Wang et al., 2012; Liu et al., 2018). Our previous work and a recent study by others have demonstrated
496 that the LysM-RLK Bti9 (also named LYK1) is the closest homology of CERK1 in tomato (Zeng et al., 2012;
497 Jaiswal et al., 2022). Bti9 RNAi-silenced plants show increased susceptibility to *Pst* specifically in older
498 leaves (Zeng et al., 2012). However, in our present epistatic analysis of an RG-pic3/RG-bti9 double
499 mutant we found that the absence of Bti9 had little effect on the enhanced resistance seen in older
500 leaves of RG-pic3 (**Supplemental Figure S10**). Moreover, we found that co-expression of Pic3 and Bti9 in
501 *N. benthamiana* leaves does not affect Bti9 phosphorylation status in plant cells (**Supplemental Figure**
502 **S11**). These observations suggest that Pic3 does not play a detectable role in Bti9-associated defense.
503 Investigation of other possible substrates of Pic3 and Pic12 will be a focus of our future work.

504 We considered the possible role of salicylic acid (SA) and abscisic acid (ABA) in Pic3-associated defense.
505 Isochorismate synthase, a key enzyme in SA biosynthesis, is encoded by the *ICS* gene which, in
506 *Arabidopsis*, is transcriptionally upregulated during many defense responses (Macaulay et al., 2017).
507 However, the transcript abundance of the single *ICS* gene that is present in tomato (Changwal et al.,
508 2021) was not significantly increased in RG-pic3 plants compared to wild-type plants after *Pst*
509 inoculation based on our RNA-seq data. Regarding ABA, no members of the PP2C clade D PP2Cs, to
510 which Pic3 and Pic12 belong, have yet been implicated in ABA signaling (Qiu et al., 2022). Additionally,
511 we observed no effect on the expression of two ABA reporter genes in the RG-pic3 mutant plants.
512 (**Supplemental Figure S5**), suggesting ABA is not involved in the enhanced resistance seen in RG-pic3
513 plants. Further research is likely needed to understand if Pic3 or Pic12 contributes to SA, ABA or other
514 immunity-associated hormone pathways during *Pst* attack.
515 Based on our current data, we propose that Pic3 and Pic12 act at the cell periphery to dephosphorylate
516 common as well as some different pattern recognition receptors (PRRs) or their downstream signaling
517 component(s) to regulate immunity. Several of our observations support this hypothesis. First, the
518 palmitoylation motifs of Pic3 and Pic12 are required for localization to the cell periphery and disruption
519 of palmitoylation motifs abolished the ability of Pic3 and Pic12 proteins to promote *Pst* growth in *N.*
520 *benthamiana* plants, suggesting they both act at or near the plasma membrane. Second, loss of either
521 Pic3 or Pic12 leads to increased resistance to *Pst*, and overexpression of either Pic3 or Pic12 (but not
522 phosphatase-inactive variants) renders *N. benthamiana* plants more susceptible to *Pst*. These responses
523 are independent of flagellin recognition, suggesting that Pic3 and Pic12 might regulate immunity

524 triggered by other PAMPs. Pic3 and Pic12 could also act on certain conserved proteins downstream of
525 PRRs. Because RG-pic3 and RG-pic12 mutants have some different defense phenotypes, it is possible
526 that they target some unique substrates. Identifying the substrates of Pic3 and Pic12 is an important
527 next step for further understanding how Pic3 and Pic12 regulate immunity at the molecular and protein
528 levels. Overall, our research has revealed a key role for two PP2C phosphatases in plant immunity and
529 sets the stage for future study of the substrates they target to negatively regulate immune responses.
530

531 **Materials and Methods**

532 **Generation of RG-pic mutant lines**

533 For each *Pic* gene, we designed one or two guide RNAs (gRNAs) targeting the exons near the 5' terminus
534 using the software Geneious R11 (Kearse et al., 2012). Each gRNA cassette was cloned into a Cas9-
535 expressing binary vector (p201N:Cas9) by Gibson assembly as described previously (Jacobs and Martin,
536 2016). The p201N:Cas9 construct carrying each gRNA was introduced into *Agrobacterium tumefaciens*
537 strain AGL1 through electroporation. For *Pic* genes that were targeted by two gRNAs, Agrobacterium
538 cells containing each gRNA/Cas9 construct were pooled together and used for transformation into the
539 tomato cultivar Rio Grande-PtoR (RG-PtoR, which has the *Pto* and *Prf* genes). Tomato transformation
540 was carried out at the Center for Plant Biotechnology Research at the Boyce Thompson Institute for
541 Plant Research. Transgenic plants were confirmed by PCR using specific primers (**Supplemental Table**
542 **S4**) and sequencing at the Biotechnology Resource Center at Cornell University. Geneious R11 and the
543 web-based tool TIDE (Tracking of Indels by Decomposition, https://tide.deskgen.com; (Brinkman et al.,
544 2014)) were used to determine the mutation type and frequency using the sequencing files (ab1
545 format).
546

547 **Off-target Mutation Detection**

548 For Pic3 and Pic12 loss-of-function mutant lines, two potential off-target sites (with the highest
549 probabilities) predicted by CRISPR-P v2 (Liu et al., 2017) were tested. Five plants from RG-pic3-1 or RG-
550 pic12-1 T3 populations were randomly selected and PCR was conducted to amplify the DNA fragments
551 that flank these predicted off-target sites using specific primers (**Supplemental Table S4**). PCR products
552 were sequenced (Sanger sequencing) and compared with reference gene sequences from the tomato
553 genome database (https://solgenomics.net). No alterations of any of the potential off-targets was
554 observed which aligns with our characterization of off-targets in a larger collection of tomato mutants
555 generated by CRISPR/Cas9 (Zhang et al., 2020).

556

557 **Disease Inoculation Assay**

558 Four- to five-week-old tomato plants (a stage showing no senescence in RG-pic3 or RG-pic12) were used
559 for disease assays. Tomato plants were submerged into a suspension of *P. syringae* pv. *tomato* strains
560 DC3000, DC3000Δ*avrPto*Δ*avrPtoB* (DC3000ΔΔ), DC3000Δ*avrPto*Δ*avrPtoB*Δ*fliC* (DC3000ΔΔΔ), or
561 *Xanthomonas euvesicatoria* strain 85-10 and the whole plant was uniformly inoculated using vacuum
562 infiltration. Inoculation titers ranged from $2x10^4$ to $1x10^7$ cfu/mL and are indicated in the figure legends.
563 Three or four plants per line were tested with each bacterial strain. Bacterial populations were
564 measured at 3 hr (for 0 days post-inoculation; dpi) and 2 dpi. Disease symptoms were photographed at 3
565 to 8 days after bacterial infection.

566

567 **Construct Generation**

568 The coding region of each gene was amplified from tomato cDNA using KOD hot start DNA polymerase
569 (Thermo Fisher Scientific) and gene-specific primers (**Supplemental Table S4**) and first cloned into
570 pENTR/D-TOPO entry vector following manufacturer's instructions (Thermo Fisher Scientific). The gene
571 expression cassette in pENTR/D-TOPO was then cloned into the destination vector pGWB414, pGWB417
572 or pGWB541 (Nakagawa et al., 2007) via recombination reactions using LR Clonase II (Thermo Fisher
573 Scientific). Vectors were confirmed by Sanger sequencing and transformed into *Agrobacterium*
574 *tumefaciens* strain 1D1249, GV2260 or GV3101 for transient expression in *N. benthamiana*.
575 Palmitoylation motifs were predicted using the online tool GPS-Palm (https://gpspalm.biocuckoo.cn/;
576 (Ning et al., 2021)). Nucleotide changes leading to amino acid substitutions for Pic3 and Pic12 were first
577 created in pENTR/D-TOPO (which contained wild-type Pic3 or Pic12) vectors by using the Q5 site-
578 directed mutagenesis kit (New England Biolabs) with specific primers (**Supplemental Table S4**). The
579 resulting mutated vectors were then cloned into the destination vector pGWB414, or pGWB541 through
580 an LR reaction.

581

582 **Agromonas Assay**

583 The agromonas assays were performed as described previously (Buscaill et al., 2021). Briefly,
584 Agrobacterium strain 1D1249 carrying a binary vector (pGWB414 or pGWB417) expressing the gene of
585 interest were syringe infiltrated into leaves of 5-week-old *N. benthamiana* plants. Two days later, the
586 same agroinfiltrated spots were syringe infiltrated with either *Pst* DC3000Δ*hopQ1-1* or DC3000Δ*hopQ1-*
587 *1ΔfliC* at $5x10^4$ cfu/mL. Bacterial populations were measured by serial dilutions on LB medium

588 supplemented with 10 µg/mL cetrimide, 10 µg/mL fucidin, and 50 µg/mL cephaloridine (CFC; Oxoid C-F-
589 C Supplement) at 2 days after *Pst* inoculation.
590
591 **Confocal Microscopy**
592 *N. benthamiana* leaves were agroinfiltrated to transiently express the protein of interest and examined
593 with a Leica TCS SP5 Laser Scanning Confocal Microscope (Leica Microsystems, Exton, PA, USA) using a
594 63x water immersion objective NA 1.2 (HCX PL APO). YFP was excited using a 488-nm laser line from an
595 argon laser line and collected between 525 nm and 550 nm using an HyD detector. Images were
596 processed using Leica LAS-AF software version 2.7.3 (Leica Microsystems). Microscopy analysis was
597 conducted at Plant Cell Imaging Center at the Boyce Thompson Institute for Plant Research.
598
599 **MAPK Phosphorylation Assay**
600 MAPK assays were performed as described previously (Zhang et al., 2020). Briefly, six leaf discs from 4-
601 week-old plants were floated in water overnight to let the wound response subside. The leaf discs were
602 then incubated in 10 nM of flg22, 25 nM of flgII-28, 50 nM of csp22 or water (negative control) for 10
603 min, and flash frozen in liquid nitrogen. Protein was extracted using a buffer containing 50mM of Tris-
604 HCl at pH 7.5, 10% (v/v) glycerol, 2mM of EDTA, 1% (v/v) Triton X-100, 5 mM of DTT (dithiothreitol), 1%
605 (v/v) protease inhibitor cocktail (Sigma-Aldrich), and 0.5% (v/v) phosphatase inhibitor cocktail 2 (Sigma-
606 Aldrich). MAPK phosphorylation was determined using an antiphospho-p44/42 MAPK (Erk1/2) antibody
607 (anti-pMAPK; Cell Signaling).
608
609 **Immunoblotting**
610 Total protein was extracted from *N. benthamiana* leaves using protein extraction buffer containing 50
611 mM Tris-HCl (pH 7.5), 10% glycerol, 150 mM NaCl, 10 mM $MgCl_2$, 5 mM EDTA, 5 mM DTT (dithiothreitol),
612 and 1% (v/v) protease inhibitor cocktail (Sigma-Aldrich). A 12 µL soluble protein solution mixed with 4 µL
613 Laemmli sample buffer was boiled at 95°C for 6 min before loading for gel electrophoresis. Protein was
614 separated by 8%–12% sodium dodecyl sulfate–polyacrylamide gel electrophoresis (SDS-PAGE) and
615 blotted on polyvinylidene difluoride membrane (Merck Millipore). The membranes were exposed to
616 anti-HA (1:5000; v/v), anti-MYC (1:10000; v/v), or anti-GFP (1:5000; v/v) primary antibody and
617 corresponding anti-rat-HRP (1:10000; v/v; for HA) or anti-mouse-HRP (1:10000; v/v; for MYC and GFP)
618 secondary antibody and developed with Pierce ECL plus substrate (Thermo Fisher Scientific) for 5 min.
619 Images were acquired by using Bio-Rad ChemiDoc Imaging system (Bio-Rad).

620

621 **Phos-tag phosphoprotein separation**

622 Phosphoprotein separation was carried out using Phos-tag SDS PAGE as described previously (Liu et al.,
623 2023) with slight modification. Briefly, total protein was extracted from *N. benthamiana* leaves (co-
624 expressing Bti9-MYC with Pic3-HA or YFP-HA proteins) using protein extraction buffer containing 50 mM
625 HEPES (4-(2-hydroxyethyl)-1-piperazineethanesulfonic acid pH 7.5), 10% glycerol, 150 mM NaCl, 50 mM
626 β-glycerophosphate, 2 mM DTT (dithiothreitol), 1% (v/v) Triton X-100, 1% (v/v) protease inhibitor
627 cocktail (Sigma-Aldrich) and 0.5% (v/v) phosphatase inhibitor cocktail 2 (Sigma-Aldrich). Protein extracts
628 were separated in an 8% SDS-PAGE gel containing 40 µM Phos-tag (Fujifilm Wako Chemicals), 150 µM
629 $MnCl_2$ and 0.38 M Tris-HCl (pH 8.4). Note that the protein ladder is incompatible with Phos-tag gel and
630 was not used in these experiments. The proteins were blotted on polyvinylidene difluoride membrane
631 (Merck Millipore) and Bti9-MYC was detected with an anti-MYC antibody.

632

633 **ROS Assay**

634 ROS production was measured as described previously (Hind et al., 2016). Briefly, leaf discs were
635 collected and floated in 200 µL water in a 96-well Nunc flat-bottom microplate overnight (16 h). Water
636 was then removed and replaced with a 100 µL solution containing 100 nM of flg22
637 (QRLSTGSRINSAKDDAAGLQIA) or 100 nM of flgII-28 (ESTNILQRMRELAVQSRNDSNSSTDRDA), in
638 combination with 34 mg/mL of luminol (Sigma-Aldrich) and 20 mg/mL of horseradish peroxidase. ROS
639 production was monitored over 45 min using a Synergy-2 microplate reader (BioTek). Three plants per
640 line and two to four discs per plant were tested in each experiment.

641

642 **qRT-PCR**

643 Wild-type 4-week-old RG-PtoR plants were vacuum infiltrated with $5x10^6$ cfu/mL
644 DC3000Δ*avrPto*Δ*avrPtoB*Δ*fliC* or 10 mM $MgCl_2$. At least three plants were used for each treatment. After
645 6 h, around 50 mg of tissue from the older (1st or 2nd) and younger (4th or 5th) leaves from each plant
646 were collected and flash frozen in liquid N_2. Total RNA was isolated using an RNeasy Plant Mini Kit
647 (Qiagen). Total RNA (about 3 µg) was treated with TURBO DNA-free DNase (Thermo Fisher Scientific) for
648 45 min at 37°C. First-strand complementary DNA was then synthesized using the above RNA via
649 SuperScript III and Oligo(dT)20 primer (Thermo Fisher Scientific). Quantitative PCR was performed with
650 specific primers (**Supplemental Table S4**) using the QuantStudio 6 Flex Real-Time PCR System (Thermo
651 Fisher Scientific) and cycling conditions for PCR were 50°C for 2 min, 95°C for 10 min, and followed by 40

652 cycles of 95°C for 30 s, 60°C for 1 min. Tomato *SlArd2* (*Solyc01g104170*) was used as the reference gene
653 (Pombo et al., 2017).
654
655 **RNA-Seq**
656 Four-week-old wild-type RG-PtoR and RG-pic3-1, RG-pic3-2 mutant plants were vacuum infiltrated with
657 $5x10^6$ cfu/mL DC3000Δ*avrPto*Δ*avrPtoB*Δ*fliC*. Six leaf discs (about 50 mg) from older (1st or 2nd) or
658 younger (4th and 5th) leaves were collected at 6 h after infiltration. Total RNA was isolated using an
659 RNeasy Plant Mini Kit (Qiagen) and then was treated with TURBO DNA-free DNase (Thermo Fisher
660 Scientific) for 45 min at 37°C. RNA libraries were prepared and sequenced on an Illumina HiSeq 4000
661 system. Raw RNA-seq reads were processed to remove adaptors and low-quality sequences using
662 Trimmomatic (version 0.39) with default parameters (Bolger, Lohse and Usadel, 2014). The remaining
663 cleaned reads were aligned to the ribosomal RNA database (Quast et al., 2013) using bowtie (version
664 1.1.2) (Langmead, 2010) allowing up to three mismatches, and those aligned were discarded. The
665 remaining cleaned reads were mapped to the tomato reference genome (SL4.0 and ITAG4.1) using
666 HISAT2 (version 2.1.0) (Kim et al., 2019) with default parameters. Based on the alignments, raw read
667 counts for each gene were calculated using HTSeq-count (Anders, Pyl and Huber, 2015) and normalized
668 to FPKM. Raw read counts were then fed to DESeq2 (Love, Huber and Anders, 2014) to identify
669 differentially expressed genes, with a cutoff of adjusted P (FDR) < 0.05 and fold change ≥2. Raw RNA-Seq
670 reads have been deposited in the NCBI BioProject database under the accession number PRJNA1079816.
671
672 **Acknowledgments**
673 We thank Tara McCrudden, Julie Bell, Kelly Jackson, Philip Ricci and Nick Vail for plant care, Joyce Van
674 Eck, Qingzhen Jiang and Tish Keen for tomato transformation, and Sergey Ivanov and Mamta Srivastava
675 for assistance with confocal imaging. JC thanks Professor Amir Sharon for supporting his research at Tel
676 Aviv University. RES was funded by NSF Research for Undergraduates award DBI-1850796. This work
677 was supported by grant IS-5362-21CR to GSe and GBM from the United States-Israel Binational
678 Agricultural Research and Development Fund (BARD). This paper is dedicated to the memory of Guido
679 Sessa.
680
681
682
683 **Author contributions**

684 FX, GSe, GSo and GBM conceived and designed the experiments. FX and NZ designed gRNAs and
685 constructed vectors. FX performed genotyping and phenotyping experiments. FX, GBM, GSe and GSo
686 analyzed the data. RS and JC helped with phenotyping experiments. XT and ZF performed RNA-Seq data
687 analysis. FX and GBM interpreted the data and wrote the manuscript. All the authors, except GSe, read
688 and approved the manuscript.
689
690 **Competing interests**
691 The authors declare that they have no conflict of interest.
692
693
694 **References**

695 **Anders S, Pyl PT, Huber W** (2015) HTSeq--a Python framework to work with high-throughput sequencing
696 data. Bioinformatics **31:** 166-169

697 **Bheri M, Mahiwal S, Sanyal SK, Pandey GK** (2021) Plant protein phosphatases: What do we know about
698 their mechanism of action? FEBS J **288:** 756-785

699 **Bi G, Zhou Z, Wang W, Li L, Rao S, Wu Y, Zhang X, Menke FLH, Chen S, Zhou JM** (2018) Receptor-Like
700 Cytoplasmic Kinases Directly Link Diverse Pattern Recognition Receptors to the Activation of
701 Mitogen-Activated Protein Kinase Cascades in Arabidopsis. Plant Cell **30:** 1543-1561

702 **Bolger AM, Lohse M, Usadel B** (2014) Trimmomatic: A flexible trimmer for Illumina sequence data.
703 Bioinformatics **30:** 2114-2120

704 **Bolton MD** (2009) Primary metabolism and plant defense--fuel for the fire. Mol Plant Microbe Interact
705 **22:** 487-497

706 **Brinkman EK, Chen T, Amendola M, van Steensel B** (2014) Easy quantitative assessment of genome
707 editing by sequence trace decomposition. Nucleic Acids Res **42:** e168

708 **Buscaill P, Sanguankiattichai N, Lee YJ, Kourelis J, Preston G, van der Hoorn RAL** (2021) Agromonas: a
709 rapid disease assay for Pseudomonas syringae growth in agroinfiltrated leaves. Plant J **105:** 831-
710 840

711 **Changwal C, Shukla T, Hussain Z, Singh N, Kar A, Singh VP, Abdin MZ, Arora A** (2021) Regulation of
712 Postharvest Tomato Fruit Ripening by Endogenous Salicylic Acid. Frontiers in Plant Science **12**

713 **Chen K, Li GJ, Bressan RA, Song CP, Zhu JK, Zhao Y** (2020) Abscisic acid dynamics, signaling, and
714 functions in plants. J Integr Plant Biol **62:** 25-54

715 **Cheng Q, Xiao H, Xiong Q** (2020) Conserved exitrons of FLAGELLIN-SENSING 2 (FLS2) across dicot plants
716 and their functions. Plant Sci **296:** 110507

717 **Chinchilla D, Bauer Z, Regenass M, Boller T, Felix G** (2006) The *Arabidopsis* receptor kinase FLS2 binds
718 flg22 and determines the specificity of flagellin perception. Plant Cell **18:** 465-476

719 **Chinchilla D, Zipfel C, Robatzek S, Kemmerling B, Nurnberger T, Jones JD, Felix G, Boller T** (2007) A
720 flagellin-induced complex of the receptor FLS2 and BAK1 initiates plant defence. Nature **448:**
721 497-500

722 **Clarke CR, Chinchilla D, Hind SR, Taguchi F, Miki R, Ichinose Y, Martin GB, Leman S, Felix G, Vinatzer BA**
723 (2013) Allelic variation in two distinct *Pseudomonas syringae* flagellin epitopes modulates the
724 strength of plant immune responses but not bacterial motility. New Phytol **200:** 847-860

725 **Conner SH, Kular G, Peggie M, Shepherd S, Schuttelkopf AW, Cohen P, Van Aalten DM** (2006) TAK1-
726 binding protein 1 is a pseudophosphatase. Biochem J **399:** 427-434

727 **Couto D, Niebergall R, Liang X, Bucherl CA, Sklenar J, Macho AP, Ntoukakis V, Derbyshire P, Altenbach**
728 **D, Maclean D, Robatzek S, Uhrig J, Menke F, Zhou JM, Zipfel C** (2016) The Arabidopsis protein
729 phosphatase PP2C38 negatively regulates the central immune kinase BIK1. PLoS Pathog **12:**
730 e1005811

731 **Danielle MS, Alba M-P, Alexandra JW, Charis R, Judith F, Ning Z, Melanie M, Gregory BM, Adam S,**
732 **Georg F, Gitta C** (2024) Natural variation of immune epitopes reveals intrabacterial antagonism.
733 bioRxiv**:** 2023.2009.2021.558511

734 **DeFalco TA, Anne P, James SR, Willoughby AC, Schwanke F, Johanndrees O, Genolet Y, Derbyshire P,**
735 **Wang Q, Rana S, Pullen AM, Menke FLH, Zipfel C, Hardtke CS, Nimchuk ZL** (2022) A conserved
736 module regulates receptor kinase signalling in immunity and development. Nat Plants **8:** 356-
737 365

738 **DeFalco TA, Zipfel C** (2021) Molecular mechanisms of early plant pattern-triggered immune signaling.
739 Mol Cell **81:** 3449-3467

740 **del Pozo O, Pedley KF, Martin GB** (2004) MAPKKKα is a positive regulator of cell death associated with
741 both plant immunity and disease. EMBO J **23:** 3072-3082

742 **Ekengren S, Liu Y, Schiff M, Dinesh-Kumar S, Martin G** (2003) Two MAPK cascades, NPR1, and TGA
743 transcription factors play a role in Pto-mediated disease resistance in tomato. Plant J **36:** 905-
744 917

745 **Erickson J, Weckwerth P, Romeis T, Lee J** (2022) What's new in protein kinase/phosphatase signalling in
746 the control of plant immunity? Essays Biochem **66:** 621-634

747 **Fuchs S, Grill E, Meskiene I, Schweighofer A** (2013) Type 2C protein phosphatases in plants. FEBS J **280:**
748 681-693

749 **Giska F, Martin GB** (2019) PP2C phosphatase Pic1 negatively regulates the phosphorylation status of
750 Pti1b kinase, a regulator of flagellin-triggered immunity in tomato. Biochem J **476:** 1621-1635

751 **Gomez-Gomez L, Bauer Z, Boller T** (2001) Both the extracellular leucine-rich repeat domain and the
752 kinase activity of FSL2 are required for flagellin binding and signaling in Arabidopsis. Plant Cell
753 **13:** 1155-1163

754 **He X, Anderson J, del Pozo O, Gu Y, Tang X, Martin G** (2004) Silencing of subfamily I of protein
755 phosphatase 2A catalytic subunits results in activation of plant defense responses and localized
756 cell death. Plant Journal **38:** 563-577

757 **Hind SR, Strickler SR, Boyle PC, Dunham DM, Bao Z, O'Doherty IM, Baccile JA, Hoki JS, Viox EG, Clarke**
758 **CR, Vinatzer BA, Schroeder FC, Martin GB** (2016) Tomato receptor FLAGELLIN-SENSING 3 binds
759 flgII-28 and activates the plant immune system. Nat Plants **2:** 16128

760 **Jackson MD, Fjeld CC, Denu JM** (2003) Probing the function of conserved residues in the
761 serine/threonine phosphatase PP2Calpha. Biochemistry **42:** 8513-8521

762 **Jacobs TB, Martin GB** (2016) High-throughput CRISPR vector construction and generation of tomato
763 hairy roots for validation of DNA modifications and experimental use. J Vis Exp **110:** doi:
764 10.3791/53843

765 **Jaiswal N, Liao CJ, Mengesha B, Han H, Lee S, Sharon A, Zhou Y, Mengiste T** (2022) Regulation of plant
766 immunity and growth by tomato receptor-like cytoplasmic kinase TRK1. New Phytol **233:** 458-
767 478

768 **Jeon JE, Kim JG, Fischer CR, Mehta N, Dufour-Schroif C, Wemmer K, Mudgett MB, Sattely E** (2020) A
769 Pathogen-Responsive Gene Cluster for Highly Modified Fatty Acids in Tomato. Cell **180:** 176-187
770 e119

771 **Jones JDG, Dangl JL** (2006) The plant immune system. Nature **444:** 323-329

772 **Kearse M, Moir R, Wilson A, Stones-Havas S, Cheung M, Sturrock S, Buxton S, Cooper A, Markowitz S,**
773 **Duran C, Thierer T, Ashton B, Meintjes P, Drummond A** (2012) Geneious Basic: an integrated
774 and extendable desktop software platform for the organization and analysis of sequence data.
775 Bioinformatics **28:** 1647-1649

776 **Kim D, Paggi JM, Park C, Bennett C, Salzberg SL** (2019) Graph-based genome alignment and genotyping
777 with HISAT2 and HISAT-genotype. Nat Biotechnol **37:** 907-915

778 **Kim YJ, Lin N-C, Martin GB** (2002) Two distinct *Pseudomonas* effector proteins interact with the Pto
779 kinase and activate plant immunity. Cell **109:** 589-598

780 **Langmead B** (2010) Aligning short sequencing reads with Bowtie. Curr Protoc Bioinformatics **Chapter 11:**
781 Unit 11 17

782 **Lei L, Zhang JY, Pu D, Liu BZ, Meng XM, Shang QM, Duan YD, Zhang F, Zhang MX, Dong CJ** (2023) ABA-
783 responsive AREB1/ABI3-1/ABI5 cascade regulates IAA oxidase gene SlDAO2 to inhibit hypocotyl
784 elongation in tomato. Plant Cell Environ **46:** 498-517

785 **Lin H** (2021) Protein cysteine palmitoylation in immunity and inflammation. FEBS J **288:** 7043-7059

786 **Lin NC, Martin GB** (2005) An *avrPto/avrPtoB* mutant of *Pseudomonas syringae* pv. tomato DC3000 does
787 not elicit Pto-mediated resistance and is less virulent on tomato. Mol Plant-Microbe Interact **18:**
788 43-51

789 **Liu J, Liu B, Chen S, Gong BQ, Chen L, Zhou Q, Xiong F, Wang M, Feng D, Li JF, Wang HB, Wang J** (2018)
790 A Tyrosine Phosphorylation Cycle Regulates Fungal Activation of a Plant Receptor Ser/Thr
791 Kinase. Cell Host Microbe **23:** 241-253 e246

792 **Love MI, Huber W, Anders S** (2014) Moderated estimation of fold change and dispersion for RNA-seq
793 data with DESeq2. Genome Biol **15:** 550

794 **Ma X, Zhang Y, Tureckova V, Xue GP, Fernie AR, Mueller-Roeber B, Balazadeh S** (2018) The NAC
795 Transcription Factor SlNAP2 Regulates Leaf Senescence and Fruit Yield in Tomato. Plant Physiol
796 **177:** 1286-1302

797 **Macaulay KM, Heath GA, Ciulli A, Murphy AM, Abell C, Carr JP, Smith AG** (2017) The biochemical
798 properties of the two Arabidopsis thaliana isochorismate synthases. Biochem J **474:** 1579-1590

799 **Mine A, Berens ML, Nobori T, Anver S, Fukumoto K, Winkelmuller TM, Takeda A, Becker D, Tsuda K**
800 (2017) Pathogen exploitation of an abscisic acid- and jasmonate-inducible MAPK phosphatase
801 and its interception by Arabidopsis immunity. Proc Natl Acad Sci U S A **114:** 7456-7461

802 **Mucyn TS, Clemente A, Andriotis VM, Balmuth AL, Oldroyd GE, Staskawicz BJ, Rathjen JP** (2006) The
803 tomato NBARC-LRR protein Prf interacts with Pto kinase *in vivo* to regulate specific plant
804 immunity. Plant Cell **18:** 2792-2806

805 **Nakagawa T, Suzuki T, Murata S, Nakamura S, Hino T, Maeo K, Tabata R, Kawai T, Tanaka K, Niwa Y,**
806 **Watanabe Y, Nakamura K, Kimura T, Ishiguro S** (2007) Improved Gateway binary vectors: high-
807 performance vectors for creation of fusion constructs in transgenic analysis of plants. Biosci
808 Biotechnol Biochem **71:** 2095-2100

809 **Ngou BPM, Ding P, Jones JDG** (2022) Thirty years of resistance: Zig-zag through the plant immune
810 system. Plant Cell **34:** 1447-1478

811 **Ning W, Jiang P, Guo Y, Wang C, Tan X, Zhang W, Peng D, Xue Y** (2021) GPS-Palm: a deep learning-
812 based graphic presentation system for the prediction of S-palmitoylation sites in proteins. Brief
813 Bioinform **22:** 1836-1847

814 **Ntoukakis V, Balmuth AL, Mucyn TS, Gutierrez JR, Jones AM, Rathjen JP** (2013) The tomato Prf complex
815 is a molecular trap for bacterial effectors based on Pto transphosphorylation. PLoS Pathog **9:**
816 e1003123

817 **Oh C-S, Martin GB** (2011) Effector-triggered immunity mediated by the Pto kinase. Trends in Plant
818 Science **16:** 132-140

819 **Oh C-S, Pedley KF, Martin GB** (2010) Tomato 14-3-3 Protein 7 Positively Regulates Immunity-Associated
820 Programmed Cell Death by Enhancing Protein Abundance and Signaling Ability of MAPKKK
821 alpha. Plant Cell **22:** 260-272

822 **Park CJ, Peng Y, Chen X, Dardick C, Ruan D, Bart R, Canlas PE, Ronald PC** (2008) Rice XB15, a protein
823 phosphatase 2C, negatively regulates cell death and XA21-mediated innate immunity. PLoS Biol
824 **6:** e231

825 **Pedley KF, Martin GB** (2003) Molecular basis of Pto-mediated resistance to bacterial speck disease in
826 tomato. Ann Rev Phytopathol **41:** 215-243

827 **Pedley KF, Martin GB** (2004) Identification of MAPKs and their possible MAPK kinase activators involved
828 in the Pto-mediated defense response of tomato. J Biol Chem **279:** 49229-49235

829 **Pombo MA, Zheng Y, Fei Z, Martin GB, Rosli HG** (2017) Use of RNA-seq data to identify and validate RT-
830 qPCR reference genes for studying the tomato-Pseudomonas pathosystem. Sci Rep **7:** 44905

831 **Pombo MA, Zheng Y, Fernandez-Pozo N, Dunham DM, Fei Z, Martin GB** (2014) Transcriptomic analysis
832 reveals tomato genes whose expression is induced specifically during effector-triggered
833 immunity and identifies the Epk1 protein kinase which is required for the host response to three
834 bacterial effector proteins. Genome Biol **15:** 492

835 **Qiu J, Ni L, Xia X, Chen S, Zhang Y, Lang M, Li M, Liu B, Pan Y, Li J, Zhang X** (2022) Genome-Wide
836 Analysis of the Protein Phosphatase 2C Genes in Tomato. Genes (Basel) **13**

837 **Quast C, Pruesse E, Yilmaz P, Gerken J, Schweer T, Yarza P, Peplies J, Glockner FO** (2013) The SILVA
838 ribosomal RNA gene database project: improved data processing and web-based tools. Nucleic
839 Acids Res **41:** D590-596

840 **Roberts R, Hind SR, Pedley KF, Diner BA, Szarzanowicz MJ, Luciano-Rosario D, Majhi BB, Popov G,**
841 **Sessa G, Oh CS, Martin G** (2019) Mai1 protein acts between host recognition of pathogen
842 effectors and mitogen-activated protein kinase signaling. Mol Plant Microbe Interact **32:** 1496-
843 1507

844 **Roberts R, Liu AE, Wan L, Geiger AM, Hind SR, Rosli HG, Martin GB** (2020) Molecular characterization of
845 differences between the tomato immune receptors Flagellin Sensing 3 and Flagellin Sensing 2.
846 Plant Physiol **183:** 1825-1837

847 **Rosli HG, Zheng Y, Pombo MA, Zhong S, Bombarely A, Fei Z, Collmer A, Martin GB** (2013)
848 Transcriptomics-based screen for genes induced by flagellin and repressed by pathogen
849 effectors identifies a cell wall-associated kinase involved in plant immunity. Genome Biol **14:**
850 R139

851 **Schultink A, Qi T, Lee A, Steinbrenner AD, Staskawicz B** (2017) Roq1 mediates recognition of the
852 *Xanthomonas* and *Pseudomonas* effector proteins XopQ and HopQ1. Plant J **92:** 787-795

853 **Schweighofer A, Hirt H, Meskiene I** (2004) Plant PP2C phosphatases: emerging functions in stress
854 signaling. Trends Plant Sci **9:** 236-243

855 **Schweighofer A, Kazanaviciute V, Scheikl E, Teige M, Doczi R, Hirt H, Schwanninger M, Kant M,**
856 **Schuurink R, Mauch F, Buchala A, Cardinale F, Meskiene I** (2007) The PP2C-type phosphatase
857 AP2C1, which negatively regulates MPK4 and MPK6, modulates innate immunity, jasmonic acid,
858 and ethylene levels in Arabidopsis. Plant Cell **19:** 2213-2224

859 **Schwizer S, Kraus CM, Dunham DM, Zheng Y, Fernandez-Pozo N, Pombo MA, Fei Z, Chakravarthy S,**
860 **Martin GB** (2017) The tomato kinase Pti1 contributes to production of reactive oxygen species in
861 response to two flagellin-derived peptides and promotes resistance to *Pseudomonas syringae*
862 infection. Mol Plant Microbe Interact **30:** 725-738

863 **Sheikh AH, Zacharia I, Pardal AJ, Dominguez-Ferreras A, Sueldo DJ, Kim JG, Balmuth A, Gutierrez JR,**
864 **Conlan BF, Ullah N, Nippe OM, Girija AM, Wu CH, Sessa G, Jones AME, Grant MR, Gifford ML,**
865 **Mudgett MB, Rathjen JP, Ntoukakis V** (2023) Dynamic changes of the Prf/Pto tomato resistance
866 complex following effector recognition. Nat Commun **14:** 2568

867 **Sobol G, Chakraborty J, Martin GB, Sessa G** (2022) The Emerging Role of PP2C Phosphatases in Tomato
868 Immunity. Mol Plant Microbe Interact **35:** 737-747

869 **Su J, Yang L, Zhu Q, Wu H, He Y, Liu Y, Xu J, Jiang D, Zhang S** (2018) Active photosynthetic inhibition
870 mediated by MPK3/MPK6 is critical to effector-triggered immunity. PLoS Biol **16:** e2004122

871 **Sun Y, Li L, Macho AP, Han Z, Hu Z, Zipfel C, Zhou JM, Chai J** (2013) Structural basis for flg22-induced
872 activation of the *Arabidopsis* FLS2-BAK1 immune complex. Science **342:** 624-628

873 **Tang X, Frederick RD, Zhou J, Halterman DA, Jia Y, Martin GB** (1996) Initiation of Plant Disease
874 Resistance by Physical Interaction of AvrPto and Pto Kinase. Science **274:** 2060-2063

875 **Tischer SV, Wunschel C, Papacek M, Kleigrewe K, Hofmann T, Christmann A, Grill E** (2017)
876 Combinatorial interaction network of abscisic acid receptors and coreceptors from Arabidopsis
877 thaliana. Proc Natl Acad Sci U S A **114:** 10280-10285

878 **Uhrig RG, Labandera AM, Moorhead GB** (2013) Arabidopsis PPP family of serine/threonine protein
879 phosphatases: many targets but few engines. Trends Plant Sci **18:** 505-513

880 **Wang C, Luan S** (2023) Calcium homeostasis and signaling in plant immunity. Curr Opin Plant Biol **77:**
881 102485

882 **Wang L, Albert M, Einig E, Furst U, Krust D, Felix G** (2016) The pattern-recognition receptor CORE of
883 Solanaceae detects bacterial cold-shock protein. Nat Plants **2:** 16185

884 **Wang WM, Ma XF, Zhang Y, Luo MC, Wang GL, Bellizzi M, Xiong XY, Xiao SY** (2012) PAPP2C interacts
885 with the atypical disease resistance protein RPW8.2 and negatively regulates salicylic acid-
886 dependent defense responses in Arabidopsis. Mol Plant **5:** 1125-1137

887 **Wei C-F, Kvitko BH, Shimizu R, Crabill E, Alfano JR, Lin N-C, Martin GB, Huang H-C, Collmer A** (2007) A
888 *Pseudomonas syringae* pv. tomato DC3000 mutant lacking the type III effector HopQ1-1 is able
889 to cause disease in the model plant *Nicotiana benthamiana*. Plant J **51:** 32-46

890 **Xue T, Wang D, Zhang S, Ehlting J, Ni F, Jakab S, Zheng C, Zhong Y** (2008) Genome-wide and expression
891 analysis of protein phosphatase 2C in rice and Arabidopsis. BMC Genomics **9:** 550

892 **Zeng L, Velasquez AC, Munkvold KR, Zhang J, Martin GB** (2012) A tomato LysM receptor-like kinase
893 promotes immunity and its kinase activity is inhibited by AvrPtoB. Plant J **69:** 92-103

894 **Zhang M, Zhang S** (2022) Mitogen-activated protein kinase cascades in plant signaling. J Integr Plant Biol
895 **64:** 301-341

896 **Zhang N, Gan J, Carneal L, Gonzalez-Tobon J, Filiatrault M, Martin GB** (2024) Helper NLRs Nrc2 and
897 Nrc3 act codependently with Prf/Pto and activate MAPK signaling to induce immunity in tomato.
898 Plant J **117:** 7-22

899 **Zhang N, Hecht C, Sun X, Fei Z, Martin GB** (2022) Loss of function of the bHLH transcription factor Nrd1
900 in tomato enhances resistance to Pseudomonas syringae. Plant Physiology **190:** 1334-1348

901 **Zhang N, Pombo MA, Rosli HG, Martin GB** (2020) Tomato Wall-Associated Kinase SlWak1 Depends on
902 Fls2/Fls3 to Promote Apoplastic Immune Responses to. Plant Physiology **183:** 1869-1882

903 **Zhang N, Roberts HM, Van Eck J, Martin GB** (2020) Generation and molecular characterization of
904 CRISPR/Cas9-induced mutations in 63 immunity-associated genes in tomato reveals specificity
905 and a range of gene modifications. Front. Plant Sci. **11:** 1-13

906 **Zhang WJ, Zhou YW, Zhang Y, Su YH, Xu TD** (2023) Protein phosphorylation: A molecular switch in plant
907 signaling. Cell Reports **42**

908 **Zipfel C, Robatzek S, Navarro L, Oakeley EJ, Jones JD, Felix G, Boller T** (2004) Bacterial disease
909 resistance in *Arabidopsis* through flagellin perception. Nature **428:** 764-767

910
911
912
913
914
915
916
917
918
919
920
921
922
923
924
925
926

927 **Figure Legends**

928

929 **Figure 1. Tomato loss-of-function RG-pic3 mutants show increased disease resistance. A)** Top panel,
930 *Pic3* gene structure including exons (red) and introns (green), arrow points to CRISPR/Cas9 gRNA target
931 site; Middle panel, sequencing chromatogram of two missense mutant alleles generated by
932 CRISPR/Cas9; Bottom panel, images of 4-week-old wild-type (Rio Grande-PtoR; RG-PtoR) and RG-pic3
933 mutant plants. **B)** Wild-type and RG-pic3 plants were vacuum-infiltrated with 5×10^4 cfu/mL
934 DC3000Δ*avrPto*Δ*avrPtoB* (DC3000ΔΔ) and photographed at 4 days post-inoculation (dpi); a section of
935 the older leaflets was enlarged for better visualization. **C)** Wild-type and RG-pic3 plants were vacuum-
936 infiltrated with 5×10^4 cfu/mL DC3000Δ*avrPto*Δ*avrPtoB*Δ*fliC* (DC3000ΔΔΔ) and photographed at 4 dpi. **D)**
937 Wild-type, RG-pic3 and RG-prf3 plants were vacuum-infiltrated with 2×10^5 cfu/mL DC3000 and
938 photographed at 4 dpi. 'Older' refers to 1st or 2nd true leaf and 'younger' refers to 4th or 5th true leaf.
939 Bacterial populations in all panels were measured at 0 and 2 dpi. Bars show means ± standard deviation,
940 n = 3 or 4. cfu, colony-forming unit. Different letters indicate significant differences based on a one-way
941 ANOVA followed by Tukey's Honest Significant Difference post hoc test ($P < 0.05$). ns, no significant
942 difference. All inoculation experiments were repeated three times with similar results.

943

944 **Figure 2. Phosphatase activity and palmitoylation motif are required for Pic3 function in defense and**
945 **palmitoylation motif affects subcellular localization of Pic3. A)** Schematic of Pic3 protein showing the
946 three predicted palmitoylation sites (red arrows) at the N terminus and two conserved aspartic acid
947 residues (green arrows) involved in metal binding in the PP2C catalytic domain. **B a**nd **C)** Leaves of 5-
948 week-old *N. benthamiana* plants were syringe-infiltrated with Agrobacterium (1D1249) strains (OD_{600}
949 = 0.6) carrying a binary expression vector (pGWB414) expressing 3× HA-tagged wild-type Pic3, a
950 phosphatase-inactive variant Pic3NN (D71N and D233N substitutions), or a Pic3SSS variant with
951 substitutions in the palmitoylation motif (C5S, C6S and C21S) or the YFP control. Two days later, the
952 same agroinfiltrated spots were syringe-infiltrated with 5×10^4 cfu /mL DC3000Δ*hopQ1-1* (B) or
953 5×10^4 cfu/mL DC3000Δ*hopQ1-1*Δ*fliC* (C). *Pst* DC3000 populations were measured at 2 days after the
954 second infiltration. Bars show means ± standard deviation, n = 4. Different letters indicate significant
955 differences based on a one-way ANOVA followed by Tukey's Honest Significant Difference post hoc test
956 ($P < 0.05$). Experiments were repeated three times with similar results. **D)** Western blotting analysis with
957 an anti-HA antibody confirmed that proteins tested in (B and C) were expressed. *N. benthamiana*
958 protein samples were collected at 40 h after initial agrobacterium infiltration. **E)** Wild-type Pic3 or the

959 Pic3SSS variant protein fused with YFP (pGWB541 vector) were transiently expressed in *N. benthamiana*
960 leaves via Agrobacterium (GV3101) for 40 h and examined under a confocal microscope. YFP
961 fluorescence was excited by 485 nm laser. The pGWB541 vector (CmR, ccdB removed) expressing YFP
962 was used as a control. Scale bar, 50 µm. Experiments were repeated twice with similar results.
963
964 **Figure 3. MAPK activation and ROS production in RG-pic3 mutant plants. A)** MAPK activation in wild-
965 type (RG-PtoR) and RG-pic3 mutant plants. Water, 10 nM flg22, 25 nM flgII-28 or 50 nM csp22 were
966 applied to detached leaf discs for 10 min and proteins were separated on 12% SDS-PAGE gel and
967 detected by an anti-pMAPK antibody. **B** and **C)** Time course of ROS production in older leaves of wild-
968 type and RG-pic3 mutant plants treated with 100 nM flg22 or 100 nM flgII-28. **D** and **E)** Time course of
969 ROS production in younger leaves of wild-type and RG-pic3 mutant plants treated with 100 nM flg22 or
970 100 nM flgII-28. ROS production was measured as relative light units (RLUs) for 45 min. Bars show
971 means ± standard deviation, n = 3 plants. An asterisk indicates significant differences between wild-type
972 and RG-pic3 plants at peak readout based on Student's t-test ($P < 0.05$), ns, no significant difference.
973 'Older' refers to 1st or 2nd true leaf and 'younger' refers to 4th or 5th true leaf. Experiments were repeated
974 three times with similar results.
975
976 **Figure 4. Enhanced disease resistance in RG-pic3 older leaves is associated with higher defense gene**
977 **expression. A)** Venn diagrams showing number of differentially-expressed genes (DEGs) in RG-pic3 and
978 wild-type plants identified through RNA-Seq. Fold change >= 2, $P < 0.05$ and FPKM (fragments per
979 kilobase of transcript per million mapped fragments) >= 3 in at least one genotype. 'Older' refers to 1st
980 or 2nd true leaf and 'younger' refers to 4th or 5th true leaf. **B)** Expression levels of several known PTI-
981 associated genes in wild-type and RG-pic3 plants older leaves at 6 h after DC3000Δ*avrPto*Δ*avrPtoB*Δ*fliC*
982 inoculation (derived from RNA-Seq data). **C)** GO-enriched terms analysis focused on up-regulated DEGs
983 in older leaves of RG-pic3 compared to that of wild-type plants. Only top 5 terms with lowest FDR (false
984 discovery rate) are shown. **D)** GO-enriched terms analysis focused on down-regulated DEGs in older
985 leaves of RG-pic3 compared to that of wild-type plants. Only the top 5 terms with lowest FDR are shown.
986 See Supplemental Table S1 for full list of significantly enriched GO terms.
987
988 **Figure 5. Tomato loss-of-function RG-pic12 mutants show increased disease resistance. A)** Top panel,
989 schematic showing gene structure of *Pic12* (Solyc10g047290) including exons (red) and introns (green),
990 arrow points to CRISPR/Cas9 gRNA target site; Middle panel, sequencing chromatogram of two missense

991 mutant alleles generated by CRISPR/Cas9; Bottom panel, images of 4-week-old wild-type (Rio Grande-
992 PtoR; RG-PtoR) and RG-pic12 mutant plants. **B)** Wild-type and RG-pic12 plants were vacuum-infiltrated
993 with 5×10^4 cfu/mL DC3000Δ*avrPto*Δ*avrPtoB* (DC3000ΔΔ), photographed at 4 days post-inoculation (dpi).
994 **C)** Wild-type and RG-pic12 plants were vacuum-infiltrated with 5×10^4 cfu/mL
995 DC3000Δ*avrPto*Δ*avrPtoB*Δ*fliC* (DC3000ΔΔΔ), and photographed at 4 dpi. **D)** Wild-type, RG-pic12 and RG-
996 prf3 plants were vacuum-infiltrated with 5×10^5 cfu/mL DC3000, and photographed at 4 dpi. 'Older'
997 refers to 1st or 2nd true leaf and 'younger' refers to 4th or 5th true leaf. Bacterial populations were
998 measured at 0 and 2 dpi. **E)** Leaves of 5-week-old *N. benthamiana* plants were syringe-infiltrated
999 with Agrobacterium (1D1249) strains (OD_{600} = 0.6) carrying a binary expression vector (pGWB414)
1000 expressing 3× HA-tagged wild-type Pic12, a phosphatase-inactive variant Pic12NN (D69N and D231N
1001 substitutions), or a Pic12SS variant with substitutions in the palmitoylation motif (C5S and C6S
1002 substitutions) or a YFP control. Two days later, the same agroinfiltrated spots were syringe-infiltrated
1003 with 5×10^4 cfu/mL DC3000*ΔhopQ1-1ΔfliC.* DC3000*ΔhopQ1-1ΔfliC* populations were measured at 2 days
1004 after the second infiltration. **F)** Western blotting analysis confirmed that proteins in (E) were expressed.
1005 Bars show means ± standard deviation, n = 3 or 4. cfu, colony-forming units. Different letters indicate
1006 significant differences based on a one-way ANOVA followed by Tukey's Honest Significant Difference
1007 post hoc test ($P < 0.05$). ANOVA was performed separately for each time point and leaf type. ns, no
1008 significant difference. Experiments (B, C and D) were repeated three times with similar results.
1009 Experiment (E) was repeated twice with similar results.
1010
1011 **Figure 6. Pic3 and Pic12 additively contribute to disease resistance to *Pst*. A)** Morphology of 4- and 8-
1012 week-old wild-type, RG-pic3-1, RG-pic12-2 and RG-pic3/RG-pic12 mutant plants. **B)** Wild-type, RG-pic3-
1013 1, RG-pic12-2 and RG-pic3/RG-pic12 plants were vacuum-infiltrated with 5×10^4 cfu/mL
1014 DC3000Δ*avrPto*Δ*avrPtoB*Δ*fliC* (DC3000ΔΔΔ). Bacterial populations were measured at 0 and 2 days post-
1015 inoculation (dpi). 'Older' refers to 1st or 2nd true leaf and 'younger' refers to 4th or 5th true leaf. Bars show
1016 means ± standard deviation, n = 4. cfu, colony-forming units. Different letters indicate significant
1017 differences based on a one-way ANOVA followed by Tukey's Honest Significant Difference post hoc test
1018 ($P < 0.05$). ANOVA was performed separately for each time point and leaf type. ns, no significant
1019 difference. **C)** Disease symptoms at 4 dpi on whole plants or the older and younger leaves of indicated
1020 genotypes related to experiment in (B). Inoculation experiments were repeated three times with similar
1021 results.
1022

1023 **Supplemental Figure Legends**

1024

1025 **Supplemental Figure S1. Summary of the mutations in the *Pic* CRISPR lines. A)** Structure of each *Pic*
1026 gene showing exons (red) and introns (green). The arrows point to the CRISPR/Cas9 gRNA target site. **B)**
1027 RG-Pic CRISPR mutant lines and detailed gRNA, mutation information. "+ 1 bp" means 1 base pair
1028 insertion and "- 1 bp" indicates 1 base pair deletion. In the RG-pic7 mutant, two PP2C genes *Pic7-03g*
1029 and *Pic7-05g* (which share high sequence similarity) were mutated via CRISPR/Cas9 guide RNA gPic7-
1030 03g-1 and gPic7-05g-1, respectively. Similarly, in the RG-pic10-1 or RG-pic10-2 mutants, two PP2C genes
1031 *Pic10-07g* and *Pic10-12g* (which share high sequence similarity) were mutated via CRISPR/Cas9 guide
1032 RNA gPic10-07g-1 and gPic10-12g-1, respectively. In all other mutants, only one PP2C *Pic* gene was
1033 edited.

1034

1035 **Supplemental Figure S2. Possible truncated proteins produced in the RG-pic3 mutants and**
1036 **morphology of 8-week-old RG-pic3 mutant plants. A)** Pic3 protein sequence in RG-PtoR (wild type) and
1037 predicted truncated proteins that might be produced as the result of a premature stop codon in RG-
1038 pic3-1 and RG-pic3-2. The deletions in the RG-pic3-1 and RG-pic3-2 plants each cause a frame shift and
1039 introduce multiple amino acid substitutions around the cut site and eventually a premature stop codon
1040 at the 35th and 63rd amino acid of the Pic3 protein, respectively. Sequence highlighted in red in RG-PtoR
1041 indicates the PP2C domain predicted by NCBI Conserved Domains website. Asterisk "*" indicates the
1042 stop codon. **B)** Morphology of 8-week-old RG-PtoR, RG-pic3-1 and RG-pic3-2 plants.

1043

1044 **Supplemental Figure S3. Loss-of-function mutations in seven tomato *Pic* genes do not affect resistance**
1045 **to *Pseudomonas syringae* pv. *tomato*. A)** Images of 4-week-old RG-PtoR (wild type) and multiple RG-pic
1046 mutant plants. **B)** RG-PtoR and RG-pic mutant plants were vacuum-infiltrated with 5×10^4 cfu/mL
1047 DC3000Δ*avrPto*Δ*avrPtoB* (DC3000ΔΔ). Bacterial populations were measured at 0 and 2 days post-
1048 inoculation (dpi). **C)** RG-PtoR and RG-pic mutant plants were vacuum-infiltrated with 5×10^4 cfu/mL
1049 DC3000Δ*avrPto*Δ*avrPtoB*Δ*fliC* (DC3000ΔΔΔ). Bacterial populations were measured at 0 and 2 dpi. **D)** RG-
1050 PtoR, RG-pic mutant and RG-prf3 plants were vacuum-infiltrated with 2×10^5 cfu/mL DC3000. Bacterial
1051 populations were measured at 0 and 2 dpi. Bars show means ± standard deviation, n = 3 or 4. cfu,
1052 colony-forming units. Different letters indicate significant differences based on a one-way ANOVA
1053 followed by Tukey's Honest Significant Difference post hoc test ($P < 0.05$). ANOVA was performed
1054 separately for each time point. ns, no significant difference. Graphs shown in (B, C and D) were made by

1055 combining results from separate small scale disease assays (i.e., from a few mutant plants). Bacterial
1056 populations of RG-PtoR from each assay were used for normalizing experimental data set. All inoculation
1057 experiments were repeated twice with similar results.
1058
1059 **Supplemental Figure S4. Loss-of-function mutation in *Pic3* does not affect the Pto/Prf3-mediated**
1060 **hypersensitive response (HR).** Wild-type (RG-PtoR), RG-pic3-1 and RG-prf3 plants (5-week-old) were
1061 vacuum-infiltrated with 1×10^7 cfu/mL DC3000 and photographed at 9 hours post-inoculation. The HR is
1062 seen as rapid leaf wilting in plants expressing Pto/Prf. RG-prf3 lacks Prf and does not develop an HR.
1063 Experiments were repeated twice with similar results.
1064
1065 **Supplemental Figure S5. Transcript levels of ABA marker genes after ABA treatment.** Expression levels
1066 of AREB1 (**A,** Solyc04g078840) and SAG113 (**B**, Solyc05g052980) in older leaves of RG-PtoR (wild type) or
1067 RG-pic3-1 plants at 0, 6 and 12 h after 100 mM abscisic acid (ABA) syringe infiltration. Bars show means
1068 ± standard deviation, n = 3 plants. P values between wild type and RG-pic3-1 were calculated using
1069 Student's t-test. Experiments were repeated twice with similar results.
1070
1071 **Supplemental Figure S6. Sequence alignment of the tomato Pic and *Arabidopsis* PP2C38 proteins.** Full
1072 length sequence of Pic and *Arabidopsis* PP2C38 (At3g12620) proteins were used to conduct alignment,
1073 only the regions near the two conserved aspartic acid residues (highlighted in red) are shown. Pic7-05g
1074 (Solyc05g052980) and Pic10-07g (Solyc07g007220) were the source sequences of Pic7 and Pic10 used in
1075 this alignment analysis.
1076
1077 **Supplemental Figure S7. Pic3 protein subcellular localization is not altered by *Pseudomonas syringae***
1078 **pv. *tomato* or flg22 treatment. A)** Western blotting analysis with an anti-YFP antibody confirmed that
1079 proteins tested in Figure 2E were expressed. *N. benthamiana* protein samples were collected at 40 h
1080 after initial Agrobacterium infiltration. **B)** Wild-type Pic3 proteins fused with YFP (pGWB541 vector)
1081 were transiently expressed in *N. benthamiana* leaves using Agrobacterium strain GV3101 for 40 h, the
1082 same Agrobacterium infiltrated spots were then syringe infiltrated with water, 1×10^7 cfu/mL
1083 DC3000*ΔhopQ1-1* or 1 µM flg22 peptide. After 1 h, the treated *N. benthamiana* leaves were examined
1084 under a confocal microscope. YFP fluorescence was excited by 485 nm laser. Scale bar, 25 µm.
1085 Experiments were repeated twice with similar results.
1086

1087 **Supplemental Figure S8. Tomato immunity-associated MAPK cascade is activated by a non-flagellin**
1088 **PAMP.** Immunoblot analysis with an anti-pMAPK antibody shows MAPK activation in RG-PtoR (wild
1089 type) and RG-pic3-1 plants by supernatants from boiled DC3000*ΔavrPtoΔavrPtoB* (DC3000ΔΔ) or
1090 DC3000*ΔavrPtoΔavrPtoBΔfliC* (DC3000ΔΔΔ). *P. s.* pv. *tomato* bacteria (1 mL of DC3000ΔΔ *or*
1091 DC3000ΔΔΔ, OD_{600} = 1.0) were boiled at 95 °C for 20 min, followed by centrifugation at 10,000 g for 5
1092 min to collect supernatant. Six leaf discs of 4-week-old plants (wild type (RG-PtoR) and RG-pic3-1) were
1093 floated in water overnight to let the wound response subside. The leaf discs were then incubated in
1094 100× diluted supernatant or water (negative control) for 10 min and phosphorylated MAPK were
1095 detected with an anti-pMAPK antibody. Numbers indicated the phosphorylated MAPK protein levels
1096 quantified using ImageJ software.
1097
1098 **Supplemental Figure S9. Expression of individual candidate genes did not alter *N. benthamiana***
1099 **disease resistance. A)** Bacterial populations in *N. benthamiana* plants transiently expressing selective
1100 RNA-seq identified tomato or YFP (control) proteins 2 days after DC3000Δ*hopQ1-1ΔfliC* infiltration.
1101 Tomato (Solyc number provided) candidate or YFP protein was fused with Myc (4×) tag using pGWB417
1102 vector. Bars show means ± standard deviation, n=4. No significant difference was detected between YFP
1103 and any of the selective RNA-seq identified proteins based on Student's t-test (P <0.05). **B)** Immunoblot
1104 analysis confirmed that proteins were expressed in (A).
1105
1106 **Supplemental Figure S10. Loss-of-function mutation in *Bti9* does not abolish enhanced resistance in**
1107 **RG-pic3 mutant. A)** Top panel, schematic showing gene structure of *Bti9* (Solyc07g049180) including
1108 exons (red) and introns (green), arrow (black) points to CRISPR/Cas9 gRNA target site; Bottom panel,
1109 sequencing chromatogram of the RG-bti9-1 mutant allele (1 bp insertion in the fourth exon) generated
1110 by CRISPR/Cas9. **B)** Wild-type, RG-pic3-1, RG-bti9-1 and RG-pic3/RG-bti9 plants were vacuum-infiltrated
1111 with 5×10^4 cfu/mL DC3000Δ*avrPtoΔavrPtoBΔfliC* (DC3000ΔΔΔ) and photographed at 3 days post-
1112 inoculation (dpi). **C)** Close-up images of the older leaves from (B). **D)** Bacterial populations in older
1113 leaves (1st or 2nd true leaf) were measured at 0 and 2 dpi. Bars show means ± standard deviation, n = 3
1114 or 4. cfu, colony-forming units. Different letters indicate significant differences based on a one-way
1115 ANOVA followed by Tukey's Honest Significant Difference post hoc test (P < 0.05). ANOVA was
1116 performed separately for each time point. ns, no significant difference. Experiments were repeated
1117 three times with similar results.
1118

1119 **Supplemental Figure S11. Pic3 does not appear to affect Bti9 phosphorylation status.** Bti9, YFP or Pic3
1120 proteins (fused with epitope tags, as shown) were transiently expressed using agroinfiltration of leaves
1121 of *N. benthamiana* with Agrobacterium strain GV2260. After 40 h, the same agroinfiltrated spots were
1122 syringe-infiltrated with either water or 200 µg/mL chitin. After 30 min, leaf samples were collected for
1123 protein extraction. Protein extracts were either separated on 12% SDS-PAGE gel and detected by an
1124 anti-Myc or anti-HA antibody or separated on 8% SDS-PAGE gel containing 40 µM Phos-tag Acrylamide
1125 AAL107 (FUJIFILM Wako Chemicals) and detected by an anti-Myc antibody. Protein extracts were
1126 treated with λ-phosphatase (NEB Lambda protein phosphatase, P0753S) following manufacturer's
1127 instructions. Arrows show the main phosphorylated proteins that were affected by λ-phosphatase.
1128 Experiment was repeated twice with similar results.
1129
1130 **Supplemental Figure S12. Pic12 and Pic3 are closely related PP2C phosphatases. A)** *Pic3* transcript
1131 abundance in leaves of RG-PtoR (wild type) plants at 6 h after mock (10 mM $MgCl_2$) or 5 ×10^6 cfu/mL
1132 DC3000*ΔavrPtoΔavrPtoBΔfliC* (DC3000ΔΔΔ) vacuum infiltration. **B)** *Pic12* transcript abundance in leaves
1133 of RG-PtoR (wild type) plants at 6 h after mock (10 mM $MgCl_2$) or 5 ×10^6 cfu/mL DC3000ΔΔΔ vacuum
1134 infiltration. 'Older' refers to 1st or 2nd true leaf and 'younger' refers to 4th or 5th true leaf. Bars show
1135 means ± standard deviation, n = 3 plants. P values between older and younger were calculated via
1136 Student's t-test. No significant difference between mock and DC3000ΔΔΔ was detected for either older
1137 or younger leaves based on Student's t-test ($P < 0.05$). **C)** Phylogenetic tree constructed using amino acid
1138 sequences of Pic3, Pic12 and related PP2C phosphatases in *Arabidopsis*, tomato and rice. Clustalx2.1 was
1139 used to conduct sequence alignment and MEGA11 was used to construct the neighbor joining
1140 phylogenetic tree, bootstrap was set as 1000. **D)** Amino acid sequence alignment between Pic3 (green)
1141 and Pic12 (red).
1142
1143 **Supplemental Figure S13. Predicted truncated proteins produced in the RG-pic12 mutants and**
1144 **morphology of 8-week-old wild type and RG-pic12 plants. A)** Pic12 amino acid sequences in RG-PtoR
1145 (wild type) and possible truncated proteins that could be produced as the result of a premature stop
1146 codon in RG-pic12-1 and RG-pic12-2. The deletions and insertions in the RG-pic12-1 and RG-pic12-2 lines
1147 cause a frameshift and introduce multiple amino acid substitutions around the cut site and eventually a
1148 premature stop codon at the 48th and 53rd amino acid of the Pic12 protein, respectively. Sequence
1149 highlighted in red in RG-PtoR indicates the PP2C domain predicted by NCBI Conserved Domains website.

1150 Asterisk "*" indicates the stop codon. **B)** Morphology of 8-week-old RG-PtoR, RG-pic12-1 and RG-pic12-2
1151 plants. **C)** Morphology of 12-week-old RG-PtoR and RG-pic12-2 plants.
1152
1153 **Supplemental Figure S14. Palmitoylation motif affects Pic12 protein subcellular localization. A)**
1154 Schematic of Pic12 protein showing the two predicted palmitoylation sites (red arrows) at the N
1155 terminus and two conserved aspartic acid residues (green arrows) involved in metal binding in the PP2C
1156 catalytic domain. **B)** Wild-type Pic12 or the Pic12SS variant protein fused with YFP (pGWB541 vector)
1157 were transiently expressed in *N. benthamiana* leaves using Agrobacterium strain GV3101 for 40 h and
1158 examined under a confocal microscope. YFP fluorescence was excited by 485 nm laser. The pGWB541
1159 vector (CmR, ccdB removed) expressing YFP was used as a control. Scale bar, 25 µm. Experiments were
1160 repeated twice with similar results. **C)** Western blotting analysis with an anti-YFP antibody confirmed
1161 that proteins tested in (B) were expressed. *N. benthamiana* protein samples were collected at 40 h after
1162 initial agrobacterium infiltration. **D)** Wild-type Pic12 protein fused with YFP (pGWB541 vector) was
1163 transiently expressed in *N. benthamiana* leaves using Agrobacterium strain GV3101 for 40 h. The same
1164 agrobacterium infiltrated spots were then syringe infiltrated with water, 1×10^7 cfu/mL DC3000*ΔhopQ1-1*
1165 or 1 µM flg22 peptide. After 1 h, the treated *N. benthamiana* leaves were examined under a confocal
1166 microscope. YFP fluorescence was excited by 485 nm laser. Scale bar, 25 µm. Experiments were
1167 repeated twice with similar results.
1168
1169 **Supplemental Figure S15. Loss-of-function mutations in *Pic12* do not affect MAPK activation or ROS**
1170 **production in response to flg22 and flgII-28. A)** MAPK activation in wild-type (RG-PtoR) and RG-pic12
1171 mutant plants. Water, 10 nM flg22 or 25 nM flgII-28 were applied to detached leaf discs for 10 min and
1172 proteins were separated on 12% SDS-PAGE gel and detected by an anti-pMAPK antibody. **B** and **C)** Time
1173 course ROS production assay in wild-type and RG-pic12 mutant plants. 100 nM flg22 or 100 nM flgII-28
1174 were used to activate ROS production in detached leaf discs and relative light units (RLUs) were
1175 measured for 45 min. Bars show means ± standard deviation, n = 3 plants. No significant differences
1176 were detected between wild-type and RG-pic12 plants at peak readout based on a one-way ANOVA
1177 followed by Tukey's Honest Significant Difference post hoc test ($P < 0.05$). Experiments were repeated
1178 three times with similar results.
1179
1180 **Supplemental Figure S16. Loss-of-function RG-pic3 and RG-pic12 mutants show enhanced disease**
1181 **resistance to *Xanthomonas euvesicatoria*. A)** Wild-type (RG-PtoR), RG-pic3-1 and RG-pic12-1 plants

1182 were vacuum-infiltrated with 2×10^5 cfu/mL *Xanthomonas euvesicatoria* strain 85-10. Bacterial
1183 populations were measured at 0 and 4 days post-inoculation (dpi). 'Older' refers to 2nd true leaf and
1184 'younger' refers to 5th true leaf. Bars show means ± standard deviation, n = 3. cfu, colony-forming units.
1185 Different letters indicate significant differences based on a one-way ANOVA followed by Tukey's Honest
1186 Significant Difference post hoc test ($P < 0.05$). ANOVA was performed separately for each time point and
1187 leaf type. ns, no significant difference. Experiments were repeated three times with similar results. **B)**
1188 Disease symptoms on younger and older leaves of indicated genotypes related to experiment in (A),
1189 photographed at 8 dpi.
1190
1191 **Supplemental Figure S17. Loss-of-function mutations in both *Pic3* and *Pic12* do not affect MAPK**
1192 **activation in response to flg22 and flgII-28.** MAPK activation in wild-type, RG-pic3-1, RG-pic12-2 and RG-
1193 pic3/RG-pic12 mutant plants. Water, 10 nM flg22 or 25 nM flgII-28 were applied to detached leaf discs
1194 for 10 min and proteins were separated on 12% SDS-PAGE gel and detected by an anti-pMAPK antibody.
1195 'Older' refers to 1st or 2nd true leaf and 'younger' refers to 4th or 5th true leaf. Experiments were repeated
1196 three times with similar results.
1197

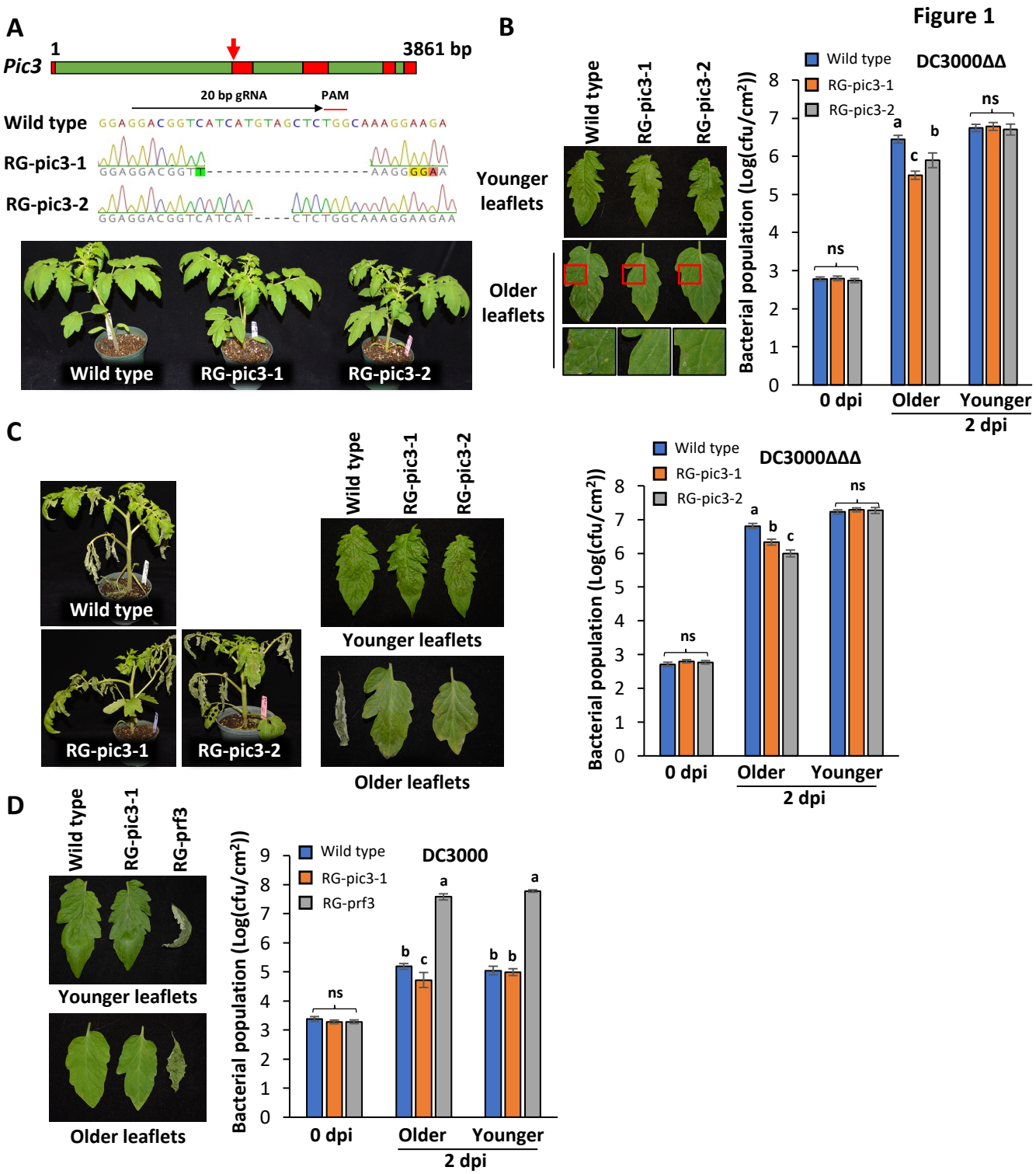

Figure 1. Tomato loss-of-function RG-pic3 mutants show increased disease resistance. A) Top panel, *Pic3* gene structure including exons (red) and introns (green), arrow points to CRISPR/Cas9 gRNA target site; Middle panel, sequencing chromatogram of two missense mutant alleles generated by CRISPR/Cas9; Bottom panel, images of 4-week-old wild-type (Rio Grande-PtoR; RG-PtoR) and RG-pic3 mutant plants. **B)** Wild-type and RG-pic3 plants were vacuum-infiltrated with 5×10^4 cfu/mL DC3000Δ*avrPto*Δ*avrPtoB* (DC3000ΔΔ) and photographed at 4 days post-inoculation (dpi); a section of the older leaflets was enlarged for better visualization. **C)** Wild-type and RG-pic3 plants were vacuum-infiltrated with 5×10^4 cfu/mL DC3000Δ*avrPto*Δ*avrPtoB*Δ*fliC* (DC3000ΔΔΔ) and photographed at 4 dpi. **D)** Wild-type, RG-pic3 and RG-prf3 plants were vacuum-infiltrated with 2×10^5 cfu/mL DC3000 and photographed at 4 dpi. 'Older' refers to 1st or 2nd true leaf and 'younger' refers to 4th or 5th true leaf. Bacterial populations in all panels were measured at 0 and 2 dpi. Bars show means ± standard deviation, n = 3 or 4. cfu, colony-forming unit. Different letters indicate significant differences based on a one-way ANOVA followed by Tukey's Honest Significant Difference post hoc test ($P < 0.05$). ns, no significant difference. All inoculation experiments were repeated three times with similar results.

Figure 2

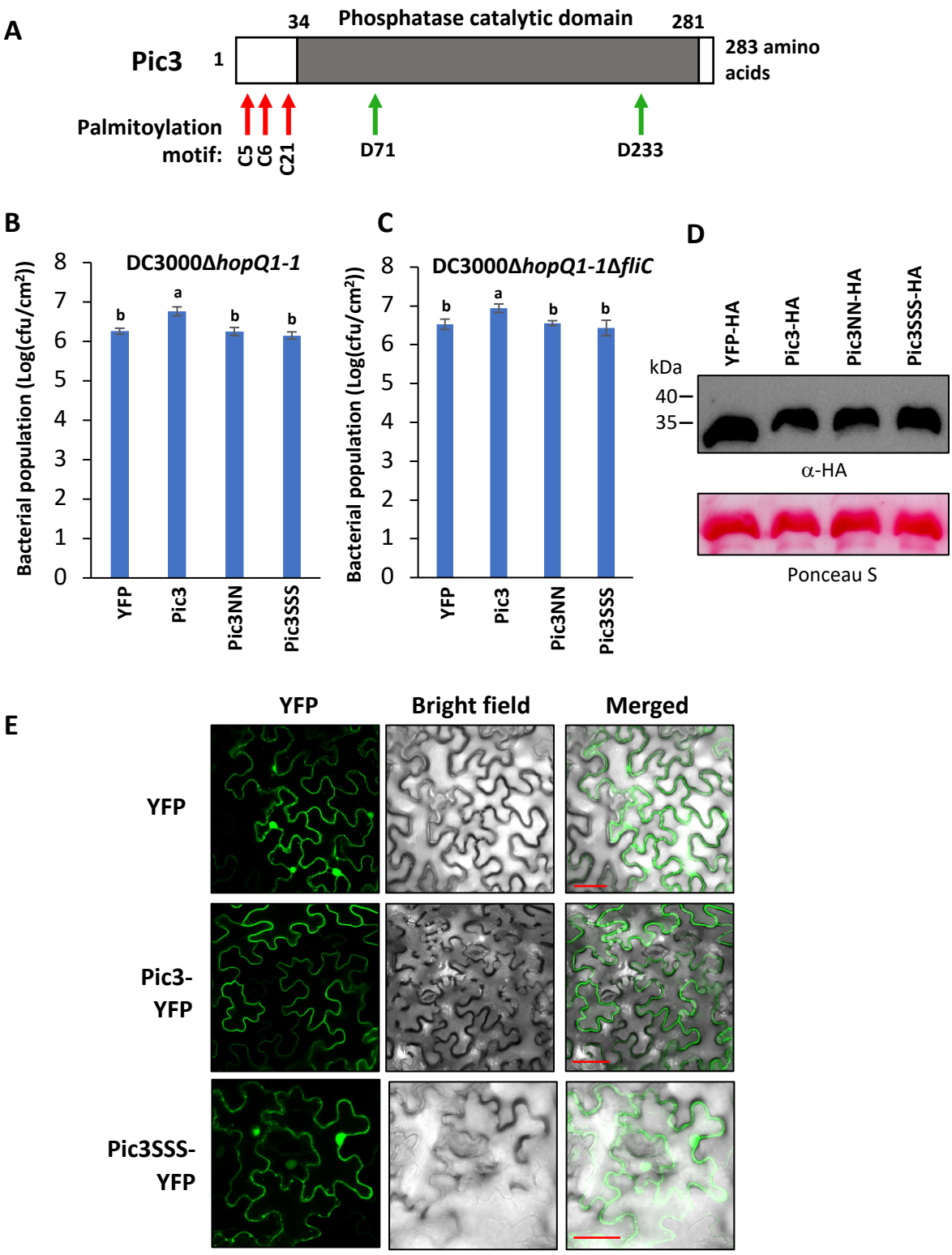
A
Pic3
1
34
Phosphatase catalytic domain
281
283 amino acids
Palmitoylation motif:
C5
C6
C21
D71
D233
B
DC3000ΔhopQ1-1
Bacterial population (Log(cfu/cm2))
YFP
Pic3
Pic3NN
Pic3SSS
C
DC3000ΔhopQ1-1ΔfliC
D
YFP-HA
Pic3-HA
Pic3NN-HA
Pic3SSS-HA
kDa
40
35
α-HA
Ponceau S
E
YFP
Bright field
Merged
Pic3-YFP
Pic3SSS-YFP

Figure 2. Phosphatase activity and palmitoylation motif are required for Pic3 function in defense and palmitoylation motif affects subcellular localization of Pic3. A) Schematic of Pic3 protein showing the three predicted palmitoylation sites (red arrows) at the N terminus and two conserved aspartic acid residues (green arrows) involved in metal binding in the PP2C catalytic domain. **B a**nd **C)** Leaves of 5-week-old *N. benthamiana* plants were syringe-infiltrated with Agrobacterium (1D1249) strains (OD_{600} = 0.6) carrying a binary expression vector (pGWB414) expressing 3× HA-tagged wild-type Pic3, a phosphatase-inactive variant Pic3NN (D71N and D233N substitutions), or a Pic3SSS variant with substitutions in the palmitoylation motif (C5S, C6S and C21S) or the YFP control. Two days later, the same agroinfiltrated spots were syringe-infiltrated with 5×10^4 cfu /mL DC3000*ΔhopQ1-1* (B) or 5×10^4 cfu/mL DC3000*ΔhopQ1-1ΔfliC* (C). *Pst* DC3000 populations were measured at 2 days after the second infiltration. Bars show means ± standard deviation, n = 4. Different letters indicate significant differences based on a one-way ANOVA followed by Tukey's Honest Significant Difference post hoc test ($P < 0.05$). Experiments were repeated three times with similar results. **D)** Western blotting analysis with an anti-HA antibody confirmed that proteins tested in (B and C) were expressed. *N. benthamiana* protein samples were collected at 40 h after initial agrobacterium infiltration. **E)** Wild-type Pic3 or the Pic3SSS variant protein fused with YFP (pGWB541 vector) were transiently expressed in *N. benthamiana* leaves via Agrobacterium (GV3101) for 40 h and examined under a confocal microscope. YFP fluorescence was excited by 485 nm laser. The pGWB541 vector (CmR, ccdB removed) expressing YFP was used as a control. Scale bar, 50 µm. Experiments were repeated twice with similar results.

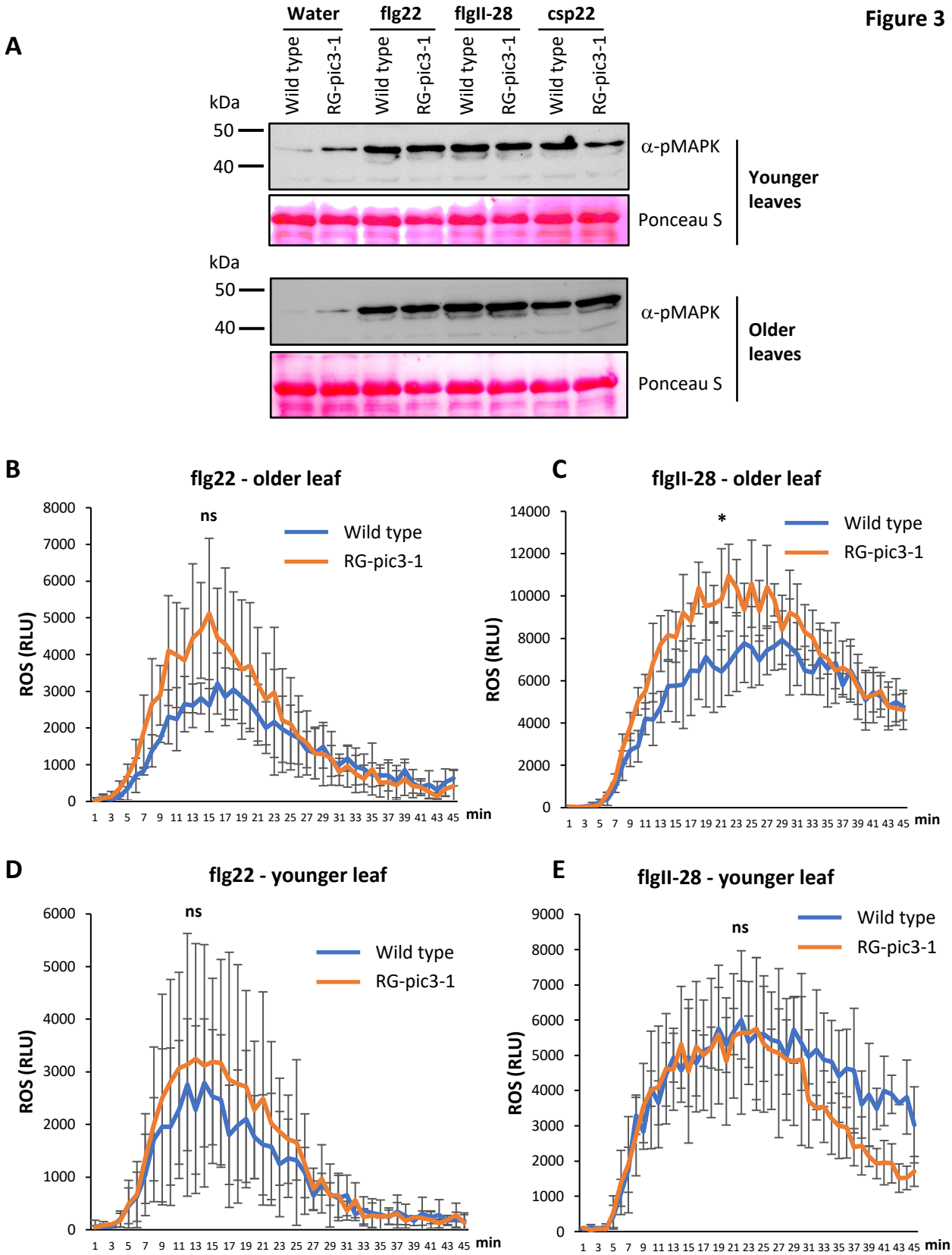

Figure 3. MAPK activation and ROS production in RG-pic3 mutant plants. A) MAPK activation in wild-type (RG-PtoR) and RG-pic3 mutant plants. Water, 10 nM flg22, 25 nM flgII-28 or 50 nM csp22 were applied to detached leaf discs for 10 min and proteins were separated on 12% SDS-PAGE gel and detected by an anti-pMAPK antibody. **B** and **C)** Time course of ROS production in older leaves of wild-type and RG-pic3 mutant plants treated with 100 nM flg22 or 100 nM flgII-28. **D** and **E)** Time course of ROS production in younger leaves of wild-type and RG-pic3 mutant plants treated with 100 nM flg22 or 100 nM flgII-28. ROS production was measured as relative light units (RLUs) for 45 min. Bars show means ± standard deviation, n = 3 plants. An asterisk indicates significant differences between wild-type and RG-pic3 plants at peak readout based on Student's t-test ($P < 0.05$), ns, no significant difference. 'Older' refers to 1st or 2nd true leaf and 'younger' refers to 4th or 5th true leaf. Experiments were repeated three times with similar results.

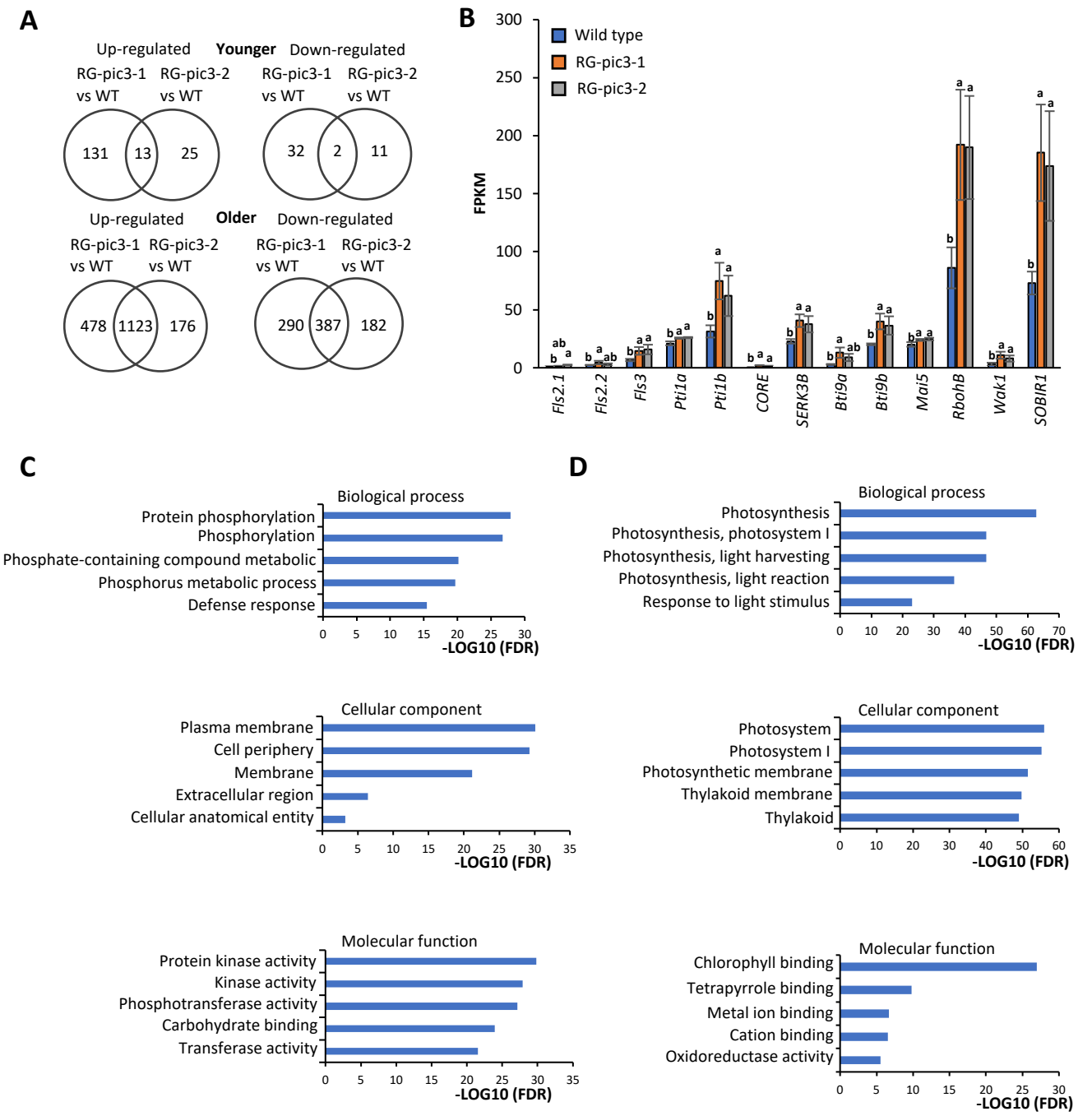

Figure 4. Enhanced disease resistance in RG-pic3 older leaves is associated with higher defense gene expression. A) Venn diagrams showing number of differentially-expressed genes (DEGs) in RG-pic3 and wild-type plants identified through RNA-Seq. Fold change >= 2, P < 0.05 and FPKM (fragments per kilobase of transcript per million mapped fragments) >= 3 in at least one genotype. 'Older' refers to 1st or 2nd true leaf and 'younger' refers to 4th or 5th true leaf. **B)** Expression levels of several known PTI-associated genes in wild-type and RG-pic3 plants older leaves at 6 h after DC3000Δ*avrPto*Δ*avrPtoB*Δ*fliC* inoculation (derived from RNA-Seq data). **C)** GO-enriched terms analysis focused on up-regulated DEGs in older leaves of RG-pic3 compared to that of wild-type plants. Only top 5 terms with lowest FDR (false discovery rate) are shown. **D)** GO-enriched terms analysis focused on down-regulated DEGs in older leaves of RG-pic3 compared to that of wild-type plants. Only the top 5 terms with lowest FDR are shown. See Supplemental Table S1 for full list of significantly enriched GO terms.

Figure 5

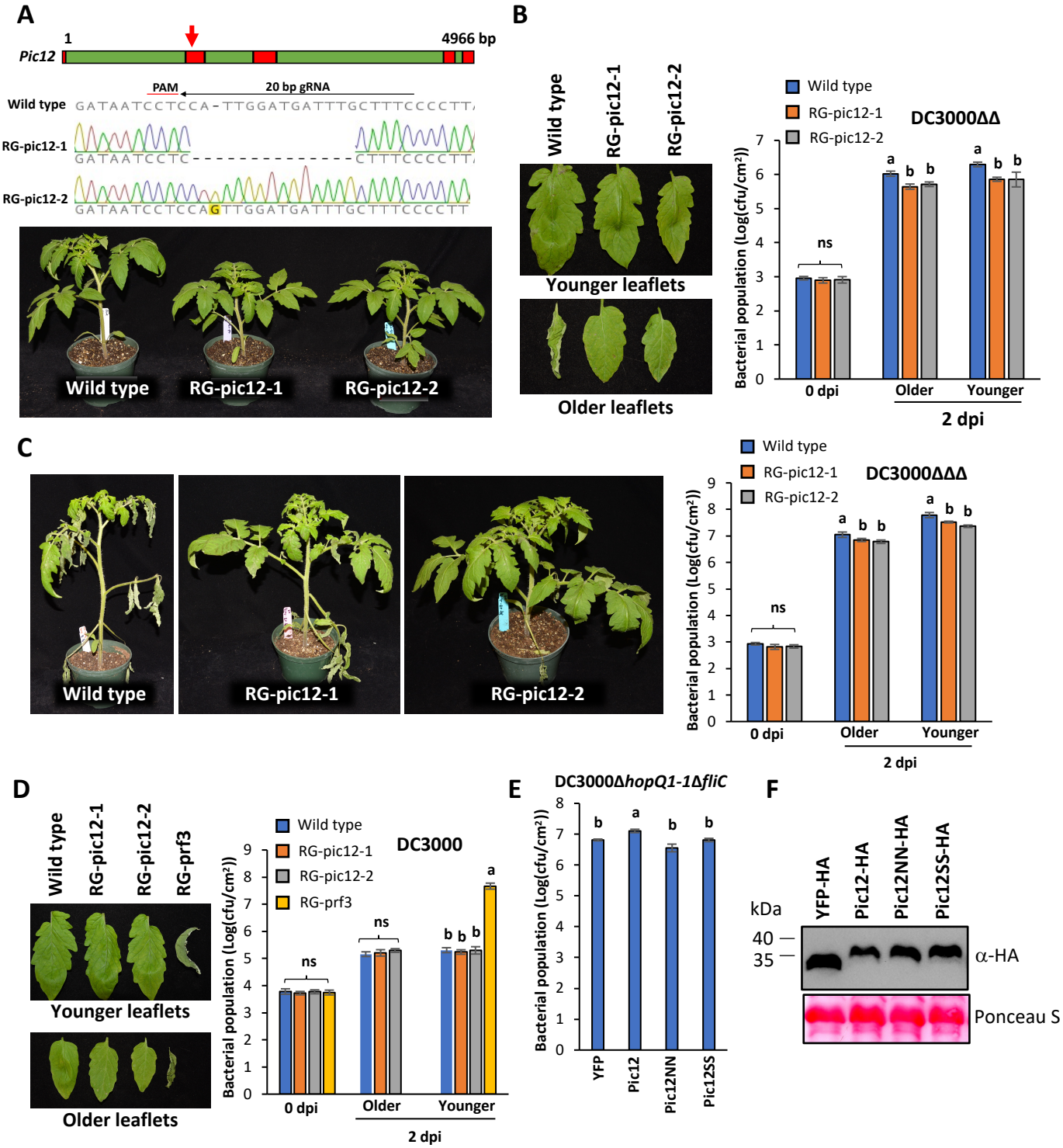
A
1
4966 bp
Pic12
PAM
20 bp gRNA
Wild type
RG-pic12-1
RG-pic12-2
GATAATCCTCCA-TTGGATGATTTGCTTTCCCCTT
GATAATCCTC
CTTTCCCCTT
GATAATCCTCCAGTTGGATGATTTGCTTTCCCCTT
Wild type
RG-pic12-1
RG-pic12-2
B
Wild type
RG-pic12-1
RG-pic12-2
Younger leaflets
Older leaflets
DC3000ΔΔ
Bacterial population (Log(cfu/cm²))
ns
0 dpi
Older
Younger
2 dpi
C
Wild type
RG-pic12-1
RG-pic12-2
DC3000ΔΔΔ
D
Wild type
RG-pic12-1
RG-pic12-2
RG-prf3
Younger leaflets
Older leaflets
DC3000
E
DC3000ΔhopQ1-1ΔfliC
YFP
Pic12
Pic12NN
Pic12SS
F
YFP-HA
Pic12-HA
Pic12NN-HA
Pic12SS-HA
kDa
40
35
α-HA
Ponceau S

Figure 5. Tomato loss-of-function RG-pic12 mutants show increased disease resistance. A) Top panel, schematic showing gene structure of *Pic12* (Solyc10g047290) including exons (red) and introns (green), arrow points to CRISPR/Cas9 gRNA target site; Middle panel, sequencing chromatogram of two missense mutant alleles generated by CRISPR/Cas9; Bottom panel, images of 4-week-old wild-type (Rio Grande-PtoR; RG-PtoR) and RG-pic12 mutant plants. **B)** Wild-type and RG-pic12 plants were vacuum-infiltrated with 5×10^4 cfu/mL DC3000Δ*avrPto*Δ*avrPtoB* (DC3000ΔΔ), photographed at 4 days post-inoculation (dpi). **C)** Wild-type and RG-pic12 plants were vacuum-infiltrated with 5×10^4 cfu/mL DC3000Δ*avrPto*Δ*avrPtoB*Δ*fliC* (DC3000ΔΔΔ), and photographed at 4 dpi. **D)** Wild-type, RG-pic12 and RG-prf3 plants were vacuum-infiltrated with 5×10^5 cfu/mL DC3000, and photographed at 4 dpi. 'Older' refers to 1st or 2nd true leaf and 'younger' refers to 4th or 5th true leaf. Bacterial populations were measured at 0 and 2 dpi. **E)** Leaves of 5-week-old *N. benthamiana* plants were syringe-infiltrated with Agrobacterium (1D1249) strains (OD_{600} = 0.6) carrying a binary expression vector (pGWB414) expressing 3× HA-tagged wild-type Pic12, a phosphatase-inactive variant Pic12NN (D69N and D231N substitutions), or a Pic12SS variant with substitutions in the palmitoylation motif (C5S and C6S substitutions) or a YFP control. Two days later, the same agroinfiltrated spots were syringe-infiltrated with 5×10^4 cfu/mL DC3000*ΔhopQ1-1ΔfliC.* DC3000*ΔhopQ1-1ΔfliC* populations were measured at 2 days after the second infiltration. **F)** Western blotting analysis confirmed that proteins in (E) were expressed. Bars show means ± standard deviation, n = 3 or 4. cfu, colony-forming units. Different letters indicate significant differences based on a one-way ANOVA followed by Tukey's Honest Significant Difference post hoc test ($P < 0.05$). ANOVA was performed separately for each time point and leaf type. ns, no significant difference. Experiments (B, C and D) were repeated three times with similar results. Experiment (E) was repeated twice with similar results.

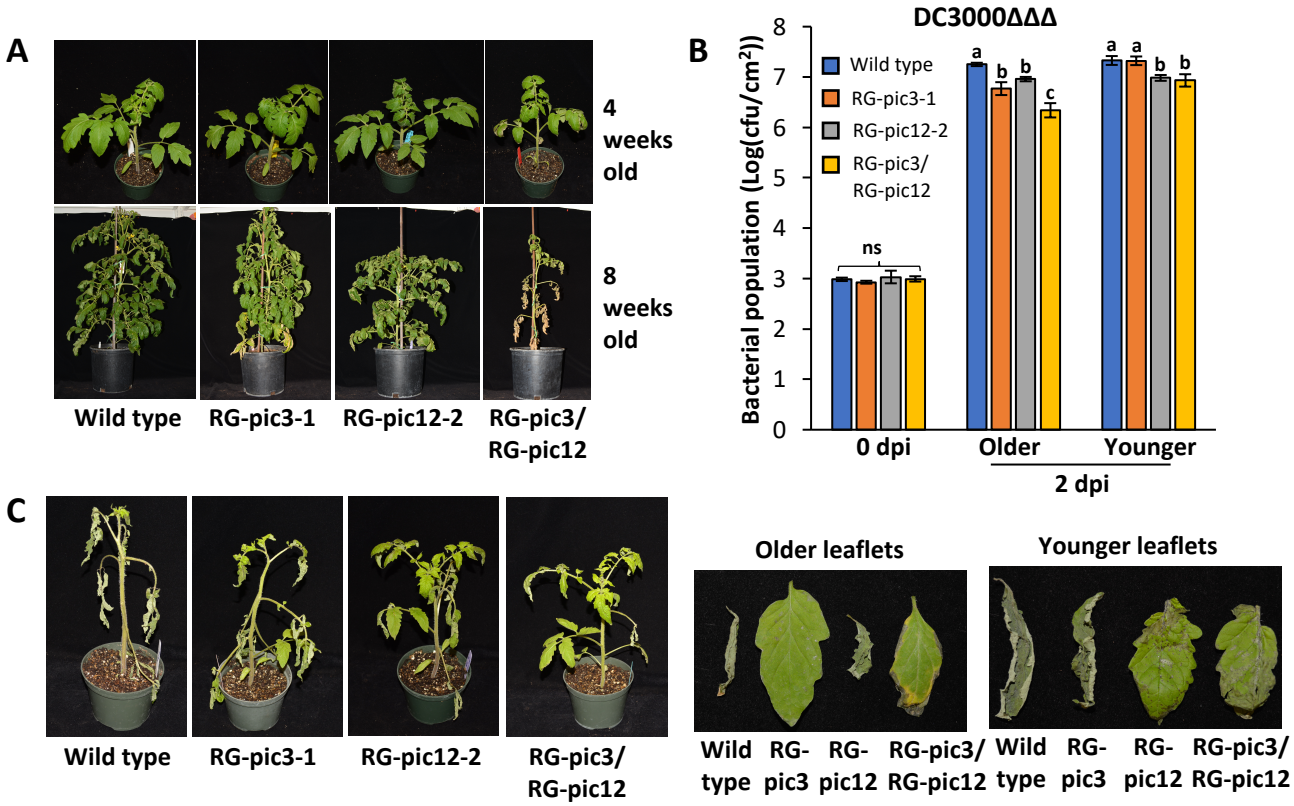

Figure 6. Pic3 and Pic12 additively contribute to disease resistance to *Pst*. A) Morphology of 4- and 8-week-old wild-type, RG-pic3-1, RG-pic12-2 and RG-pic3/RG-pic12 mutant plants. **B)** Wild-type, RG-pic3-1, RG-pic12-2 and RG-pic3/RG-pic12 plants were vacuum-infiltrated with 5×10^4 cfu/mL DC3000Δ*avrPto*Δ*avrPtoB*Δ*fliC* (DC3000ΔΔΔ). Bacterial populations were measured at 0 and 2 days post-inoculation (dpi). 'Older' refers to 1st or 2nd true leaf and 'younger' refers to 4th or 5th true leaf. Bars show means ± standard deviation, n = 4. cfu, colony-forming units. Different letters indicate significant differences based on a one-way ANOVA followed by Tukey's Honest Significant Difference post hoc test ($P < 0.05$). ANOVA was performed separately for each time point and leaf type. ns, no significant difference. **C)** Disease symptoms at 4 dpi on whole plants or the older and younger leaves of indicated genotypes related to experiment in (B). Inoculation experiments were repeated three times with similar results.